Manufacture and characterisation of PLA biocomposites with high purity cellulose isolated from olive pruning waste

José A. Rodríguez-Liébana[1], Francisco J. Navas-Martos[1*], Sofía Jurado-Contreras[2], Francisca Morillas-Gutiérrez[2], Soledad Mateo[2], Alberto J. Moya[2], M. Dolores La Rubia[2]

[1]Centro Tecnológico del Plástico. Fundación Andaltec I+D+i. Polígono Industrial Cañada de la Fuente, C/ Vilches 34, 23600 Martos (Jaén)

[2]Department of Chemical, Environmental and Materials Engineering. Campus Las Lagunillas. Universidad de Jaén 23071 (Jaén)

Abstract

In this work, a two-step chemical process was carried out on olive pruning residues according to an optimised sequence that led to the isolation of natural fibre with a high cellulose content. Reaction time, temperature and HNO_3 concentration in the acid hydrolysis stage were optimised by means of the Response Surface Methodology (RSM) to achieve the highest removal of hemicellulose and lignin and the highest crystallinity index, minimising cellulose hydrolysis. The optimum conditions were established at 240 min, 90 °C and 8%w/v acid concentration. Subsequent hydrolysis with NaOH allowed to obtain a pulp enriched in cellulose (83.28 wt.%). Analysis revealed that the cellulose isolated had a high crystallinity index (70.06%) and thermal stability (T_{max} = 357 °C). The cellulose obtained was finally used for the manufacture of polymer biocomposites and to evaluate its viability as a filler for polymeric materials. The selected polymer matrix used was acid polylactic (PLA) and the amount of filler was 5 and 15% by weight, respectively. In order to determine the influence of the cellulose purification process, the manufacture of bicomposites with untreated olive tree pruning fibre was also carried out. Finally, all the manufactured biocomposites were characterised, obtaining an increase in tensile

strength when a 15wt.% of reinforcement was added, better matrix-fibre cohesion and hydrophilicity with chemically treated fibre was used, and maintaining the melting temperature of materials remained stable.

Key-words: Olive waste, lignocellulose, biomass, hydrolysis, cellulosic fibre, biocomposites, RSM.

1. Introduction

Vegetal biomass is composed mainly by hemicellulose, lignin and cellulose, the latter being of paramount importance due to its wide range of applications in industry [1][2]. Cellulose is classically referred as a renewable and biodegradable polymer abundant in nature [1][3]. To recover cellulose from vegetal biomass, it is necessary to remove the hemicellulose and lignin. In particular, as lignin binds more strongly to cellulosic fibres and prevents cellulose from chemical attack, cellulose isolation methods have primarily focused on delignification strategies. The harsh processing conditions, as well as the environmental implications associated with the most widely used industrial processes (Kraft pulping and Organosolv) have led to the search for more sustainable methods in the last years. For instance, Tezcan and Atici (2017) achieved a cellulose enrichment from 30 to 81 wt.% and a delignification of 84 wt.% by stacking in a pile lignocellulosic bio-wastes (fall leaves) that were irrigated with a NaOH solution [2]. In addition, microcrystalline cellulose has recently been extracted from waste cotton fabrics by using a hydrothermal process in which water not only acts as a reactant but also as a catalyst, hence allowing for relatively low energy consumption [4]. However, these methods can be time consuming or difficult to implement in industry.

Acidified sodium chlorite treatment has been reported as the first step in delignification of lignocellulosic biomass [5][6]. However, repeated steps are frequently needed for the

delignification to be effective [6]. Moreover, the high environmental risks associated to the use of chlorine chemicals have stem the search for more sustainable alternatives such as hydrolysis with dilute acids [7]. In addition, by selecting the appropriate operating conditions, acid hydrolysis allows to obtain some advantages over other treatments such as low cost and the possibility of operating with dilute concentrations, thus reducing the environmental impact [8]. Regarding the selection of reagents, HNO_3 constitutes one of the best options since when the process is carried out under optimal conditions, the necessary reaction time is less than when using H_2SO_4 or HCl [9]. In this sense, HNO_3 has been reported as an effective chemical for both the pre-treatment of lignocellulosic biomass before pulping [9][10][11] and for the purification of the cellulose pulp [7][12][13]. Alternatively, a residue with a high cellulose content can be obtained by combining acid and alkaline treatments. The first step comprises the acid hydrolysis of lignocellulosic biomass to mainly remove hemicellulose, and the second step uses an alkaline agent to extract lignin [14][15].

Conditioning the olive trees after harvesting by properly trimming their branches is essential to maximise both crop productivity and life cycle of the plant. In alignment with the greener practices of modern agriculture, the valorisation of agricultural wastes, such as olive tree pruning (OTP), for different applications is ever more frequently being conceived in the waste management systems of agricultural exploitations. It is estimated that trimming of olive trees to increase crop productivity produces a volume of OTP biomass of around 2000-3000 kg ha^{-1}. As a consequence of the intense olive oil production, large amounts of OTP biomass are generated as a by-product in olive orchards every year in Spain, especially in the region of Andalusia (south of Spain) that maintains a practically constant olive grove area that exceeds 1500000 ha. Despite that the use of OTP for electricity generation has experienced a significant increase in the last decade,

this by-product is being underutilised. It is estimated that the current use of this type of biomass only reaches 30% of its full potential with great differences among geographical areas, which determines that in some regions its use is non-existent. Therefore, burning in the own orchards and soil amendment remain the only options for farmers in those areas without access to biomass power plants [16].

Few studies have been reported to date in which the isolation of cellulose from olive tree pruning residue (OTP) has been carried out, obtaining a high percentage of cellulose in the final product. Njeh et al. (2022), carried out the isolation of the cellulose from the OTP residue by means of an alkaline treatment followed by bleaching, obtaining a final product with a maximum crystallinity of up to 40% [17]. Kian et al. (2020) managed to obtain a final product with a cellulose content of up to 80%, reversing the order of the previous treatments, detecting a hemicellulose content close to 10% [5]. Another study reported the performance of a treatment to obtain microcrystalline cellulose (MCC) by means of basic and acid hydrolysis and bleaching, obtaining a cellulose with high crystallinity (74%) [18].

In recent years, polymeric composites reinforced with natural fibres have gained great importance due to their more environmentally friendly properties, their mechanical properties and relatively low production costs, among others [19]. Kumar et al. (2022) studied the effect of incorporating bamboo plant fibres as a reinforcement on the properties of a PLA polymer matrix [20]. Fico et al. (2022) carried out a study for the manufacture of a suitable PLA-based filament reinforced with between 10wt. % and a 20wt. % of olive wood powder (OW), reporting a decrease in flexural properties due to poor adhesion between the OW and the polymeric matrix [21]. Other authors have analysed the properties of hybrid composites resulting from incorporating OTP fibres and lemon fibres in a polypropylene and polyethylene matrix, and their feasibility in structural

applications [22]. Sarmin et al. (2022) carried out the manufacture and characterisation of some hybrid composites using olive waste and bamboo fibres as reinforcement, and epoxy resin as polymeric matrix [23].

Cellulose fibres have received special attention due to their contribution to the stability of thermal behaviour, the improvement of the tensile strength of biocomposites and their biocompatibility with the polymeric matrix [18]. Some works reported promising results, in terms of improving mechanical properties and increasing tensile strength, by introducing lignocellulosic reinforcements with a high cellulose content in a PLA polymer matrix [24]. Norizan et al. (2022) studied the thermal properties of PLA/cellulose composites, concluding that cellulose acts as a nucleation agent, increasing the crystallization rate and improving the thermal properties of the composite material [25]. However, no study has been found that has focused specifically on the incorporation of olive pruning wood residues with a high cellulose content into polymer matrices. As OTP biomass is clearly underutilised for industrial purposes, this work aims to the isolation of a high-purity cellulosic fraction by a simple two-step hydrolysis reaction consisting of diluted HNO_3 hydrolysis followed by alkaline treatment, thus avoiding the implementation of a bleaching step. The optimum experimental conditions of the acid reaction (time, temperature and acid concentration) to maximise the hydrolysis of hemicellulose and lignin and minimise that for cellulose were identified using Response Surface Methodology (RSM). Afterwards, the fibres obtained were further hydrolysed with NaOH to obtain a high-purity cellulosic residue. Finally, this treated residue was used as reinforcement for the fabrication of PLA-based biocomposites and examining their mechanical and thermal properties.

2. Materials and methods

2.1. Materials

125 OTP biomass was collected from a cultivation area located near the town of Martos (Jaén,
126 South Spain) in March 2021 coinciding with the pruning season. In this research, the
127 branches accumulated after pruning a large number of 15-20 years old olive trees were
128 selected. HNO_3 (Puriss. p.a., 65-67%) and NaOH pellets (≥ 99%), used for the hydrolysis
129 reactions, and H_2SO_4 (72% w/w aqueous solution), used for the chemical characterisation
130 of the fibres, were purchased from DICSA S.L. (Spain). Ingeo™ Biopolymer 3251D PLA
131 (NatureWorks LLC, United States) was selected as the polymer matrix to be used in the
132 manufacture of the biocomposites mainly due to its good balance in terms of properties
133 for compounding and injection moulding.

134 *2.2. Conditioning of OTP biomass*

135 To obtain a biomass composed of wood fibres with a particle size within an appropriate
136 range, the branches were subsequently subjected to the following conditioning process.
137 Firstly, the dry branches were processed "in situ" on the farm by using a PMA-CR series
138 pruning shredder (PROMAGRI, La Carlota, Spain) to reduce their size to a maximum
139 length of 30-40 cm. This facilitated their transportation, as well as removed most of the
140 leaves. The rest of the leaves that remained in the biomass were manually removed from
141 the wood. The resulting product was then processed in a wood chipper (Arborist 150
142 model; GreenMech Ltd., Alcester, UK) to adapt the size of the branches up to a maximum
143 length of 20 cm. Afterwards, these short-length branches were milled (SM11 model
144 cutting mill; Retsch Mühle Dietz-Motoren GmbH & Co. KG, Hann, Germany) and sieved
145 (Vibro model sieve shaker; Retsch GmbH & Co. KG, Hann, Germany) in the laboratory
146 through a previously optimised process that allowed to remove undesired fractions and to
147 obtain the maximum percentage of the final fibre within the target particle size range [26].
148 More specifically, those fibres retained in the space located between the sieves with 0.425
149 mm and 0.600 mm of nominal aperture were selected.

2.3. Isolation of cellulose from OTP biomass

The extraction of cellulose from OTP biomass was achieved by a two-step process consisting of acid hydrolysis followed by alkaline hydrolysis. Both hydrolysis treatments, described below, were carried out under mechanical stirring in a 1000 cm^3 glass reactor to which the solution, acidic or alkaline, and the selected OTP fibres were added at a solid/liquid ratio 1:10 (w/w).

2.3.1. Acid Hydrolysis (AH). Optimisation of experimental conditions.

The acid treatment was carried out with HNO_3 at different concentrations, and at varied reaction time and temperature conditions (Table 1). Once the hydrolysis was completed, the resulting solid fraction was separated by filtration, washed with abundant water to remove excess acid, dried at room temperature, and stored in zipped bags until analysis. For convenience, OTP biomass after the acid hydrolysis was labelled as OTP-AH. The yield of the acid hydrolysis reaction ($Yield_{AH}$) was calculated as:

$$Yield_{AH}(\%) = \frac{m_{OTP-AH}}{m_{OTP}} \times 100 \qquad \text{Eq. (1)}$$

where m_{OTP} and $m_{OTP\text{-}AH}$ are the weight (g) of OTP biomass before and after hydrolysis respectively.

Aimed to remove as much hemicellulose and lignin as possible and to obtain a biomass enriched in cellulose, RSM was applied to determine the best experimental conditions for the variables studied: reaction time (t), reaction temperature (T), and HNO_3 concentration (c). The approach used consisted of a face-centred central composite design (FCCD) with 17 runs including three replicates in the central point ($AH_{1\text{-}17}$). Table 1 shows the resulting matrix for the design of experiments (DOE), including both the coded and real values of the three independent variables. On the other hand, the percentages of cellulose, hemicellulose and lignin hydrolysed (Y_{cell}, Y_{hemi} and Y_{lig}) (calculated as the difference

between their contents in the OTP biomass before and after the AH process (see section 2.4.2), as well as its crystallinity index (*CrI*) calculated by X-Ray Diffraction (XRD) as in section 2.4.5 were used as the response variables. Both the numerical and graphical analysis of the results obtained were performed by means of both STATISTICA v8.0 (Statsoft, Tulsa, US) and Design-Expert v6.0 (Stat-Ease, Inc., Minneapolis, US) softwares. The relationship between the response functions and the coded variables is described by the following second-degree polynomial equation:

$$Y = \beta_0 + \beta_i \sum x_i + \beta_{ii} \sum x_i^2 + \beta_{ij} \sum x_i x_j \quad \text{Eq. (2)}$$

where Y is the specific response function, x_i and x_j are independent variables, β_0 is a constant, and β_i, β_{ii}, and β_{ij} are linear, quadratic, and interactive coefficients respectively.

2.3.2. Alkaline Hydrolysis (BH)

Once the best experimental conditions for AH were selected, the resulting biomass, depleted in hemicellulose and lignin, was further hydrolysed by following an alkaline reaction with NaOH. In this case, two different working conditions were assessed: i) NaOH 2% w/v, at 60 °C for 90 min (BH_1); and ii) NaOH 6% w/v, at 75 °C for 105 min (BH_2). As for AH process, the fully hydrolysed biomass (OTP-BH) was filtered, washed with water until reaching neutral pH, dried at room temperature, and properly stored until being characterised. In addition, the yield of the alkaline reaction ($Yield_{BH}$) was calculated with the formula:

$$Yield_{BH}(\%) = \frac{m_{OTP-BH}}{m_{OTP-AH}} \times 100 \quad \text{Eq. (3)}$$

where $m_{OTP\text{-}AH}$ is the weight (g) of OTP biomass after the AH reaction selected as optimal, and $m_{OTP\text{-}BH}$ the weight (g) of OTP biomass after the BH treatment.

2.4. Characterisation of OTP biomass at each stage of treatment

197 *2.4.1. Moisture and ash contents*

198 The moisture and ash contents of biomass samples (OTP, OTP-AH and OTP-BH) were
199 determined according to the methods reported by the Technical Association of Pulp and
200 Paper Industry (TAPPI T 12 os-75 and TAPPI T 15 os-58 respectively). The process
201 consisted in drying 1 g of sample in an oven at 105 °C until constant weight. Then, the
202 dried sample is introduced in a muffle furnace and incinerated at 600 °C for 4h. Moisture
203 and ash contents were calculated in accordance with the following equations:

204 $$Moisture\ (wt.\%) = \frac{m - m_{105}}{m} \times 100 \qquad \text{Eq. (4)}$$

205 $$Ash\ (wt.\%) = \frac{m - m_{600}}{m} \times 100 \qquad \text{Eq. (5)}$$

206 where m is the weight (g) of the sample (~1 g), m_{105} is the weight of dried OTP, and m_{600}
207 is the weight (g) of the ash obtained after incineration.

208 *2.4.2. Chemical composition*

209 The chemical composition of OTP, OTP-AH and OTP-BH fibres was determined in
210 duplicate following the methodology proposed by Browning [27] with some
211 modifications. The procedure consisted of hydrolysing 2 g of sample in 10 mL of a 72
212 %w/w H_2SO_4 solution under gentle stirring for 7 min using a 50 mL flask immersed in a
213 water bath at 60 ºC. Subsequently, 275 mL of distilled water was carefully added to dilute
214 the acid, and the solution was immediately transferred to a 1 L Erlenmeyer flask. The
215 flask was suitably sealed and autoclaved (model AE-110-DRY, RAYPA) at 1.11 atm and
216 121 °C for 45 min. The resulting solution (hydrolysate) was then cooled at room
217 temperature and filtered by using a fluted filter paper. The solid residue was washed with
218 distilled water, and the final volume of the filtrate + washing water was adjusted to 500
219 mL with a volumetric flask. Both the solid residue and the hydrolysate were used for
220 different analyses as described below.

The different hydrolysates obtained were used for the determination of carbohydrates (D-glucose, D-xylose and L-arabinose) by injecting a 20-µL aliquot of filtered sample (0.22 µm nylon syringe filters; Branchia) in a High Performance Liquid Chromatography (HPLC) system (Shimadzu Prominence Series 20) equipped with a cooled automatic sampler (SIL-20ACHT) and a refraction index detector (RID-10A). The chromatographic separation of the analytes was carried out in an Aminex HPX-87H column (300 x 7.8 mm) (Bio-Rad Laboratories Ltd.) at an oven temperature of 45 °C by using 0.005M H_2SO_4 in isocratic mode at a flow rate of 0.6 mL min^{-1} as mobile phase. The mathematical expressions proposed in [28] were used to calculate the percentages of cellulose and hemicellulose in the biomass on a dry weight basis.

On the other hand, the solid residue was used for the determination of acid insoluble or Klason lignin as in [29]. The residue was dried at 105 °C until constant weight and incinerated in a muffle furnace at 600 °C for 4 h to rule out likely interferences produced by the presence of ashes. The percentage of acid insoluble lignin in OTP samples (d.w.) was calculated following the equation:

$$Klason\ Lignin\ (wt.\%) = \frac{m_{105} - m_{600}}{m_{OTP}} \times 100 \qquad \text{Eq. (6)}$$

where m_{105} is the weight (g) of the dried solid residue, m_{600} is the weight (g) of the ash obtained after incineration, and m_{OTP} is the weight of the corresponding dried OTP biomass (~2 g).

2.4.3. Scanning Electron Microscopy

Field Emission Scanning Electron Microscopy (FE-SEM) (model Merlin, Carl Zeiss) was used to observe the surface morphology of OTP fibres. Furthermore, the effects of the chemical treatments on the morphological features of the fibres were evaluated by comparing the micrographs of untreated OTP, after AH and after BH. Biomass fibres

were placed on the sample stub, dried in an oven at 60 °C for 2 h and coated with gold using a vacuum sputter coater (model Q150T ES, Quorum Technologies). The analysis of the samples was performed at an accelerating voltage of 15 kV.

2.4.4. Fourier Transformed Infrared (FTIR) Spectroscopy

The identification of functional groups in the biomass samples and the chemical changes produced after the hydrolysis treatments were assessed by Fourier Transformed Infrared (FTIR) spectroscopy (Tensor 27 spectrophotometer, Bruker). Prior to the analysis, the samples were milled and forced to pass a 0.5 mm sieve (Ultra Centrifugal Mill ZM 200; Retsch). The FTIR spectra were recorded in 4000-400 cm^{-1} range with a resolution of 4 cm^{-1} and an accumulation of 32 scans. All the analyses were carried out in the Attenuated Total Reflection (ATR) mode.

2.4.5. X-Ray Diffraction (XRD)

In order to determine the crystallinity of OTP, OTP-AH and OTP-BH fibres, the samples were analysed by XRD technique with an Empyrean X-Ray diffractometer (Malvern PANalytical, United Kingdom). In addition, X-ray diffractograms were used to monitor the efficiency of the cellulose isolation process. Each material was milled and passed through a 0.5 mm sieve prior to the analysis (Ultra Centrifugal Mill ZM 200; Retsch). Powdered samples were placed on the sample holder and levelled to obtain total and even X-ray exposure. The samples were scanned at room temperature with a monochromatic Cu-Kα radiation source in the 2θ range of 5-40°, at a rate of 2° min^{-1} and a total scanning time of 17.5 min. The *CrI* values of the different samples were determined in accordance with the methodology proposed in [30] as below:

$$CrI\ (\%) = \frac{I_{002} - I_{am}}{I_{002}} \times 100 \qquad \text{Eq. (7)}$$

where I_{002} is the maximum intensity of the (002) lattice diffraction peak corresponding to both amorphous and crystalline phases, and I_{am} represents the intensity scattered by the amorphous part. Both I_{002} and I_{am} are located at 2θ values approximately of 22° and 18° respectively [31][32][33].

2.4.6. Thermogravimetric Analysis (TGA)

The thermal stability of the different fibres was determined in a thermogravimetric analyser (TGA Q500; TA Instruments) by weighing 10-20 mg of powdered sample in alumina pans. All the measurements were carried out under nitrogen atmosphere at a flow of 50 mL min^{-1} by heating the sample from room temperature to 1000 °C at a rate of 10 °C min^{-1}.

2.5. Preparation of biocomposites

BYK MAX-P 4101 (BYK-Chemie GmbH, Germany) was also used as process additive (PA) in order to improve the compounding manufacturing process [34]. Prior to preparing the biocomposites, moisture was removed from both the treated ($OTPBH_2$) and the non-treated OTP, drying them in an oven for 24 h at 60 as previously reported in other research papers [5]. PLA pellets were dried in a KKT 75 dryer (KOCH, Germany) under the following conditions: 45 ºC for 5 h. The biocomposites were manufactured using two different percentages of OTP, 5 and 15% by weight. Raw PLA and composition of the different manufactured biocomposites are shown in Table 2. The compounding process was carried out on a Mini E-Lab 22 extrusion-pelletizing production line (Eur.Ex.Ma, Italy), using the parameters detailed in Table 2 to finally obtain the final materials referenced in Table 2, PLA and biocomposites in the form of pellets. The control material, raw PLA, was also processed on the extrusion line under the same conditions as the biocomposite compounding process (Table 3) in order to obtain a suitable reference for comparison.

293 **Table 2.** PLA and biocomposites composition

Reference	PLA (wt.%)	OTP (wt.%)	$OTPBH_2$ (wt.%)	PA (wt.%)
PLA (Control)	98.5	-	-	1.5
5OTP/PLA	93.5	5.0	-	1.5
$5OTPBH_2$/PLA	93.5	-	5.0	1.5
15OTP/PLA	83.5	15.0	-	1.5
$15OTPBH_2$/PLA	83.5	-	15.0	1.5

294

295 **Table 3.** Compounding process parameters

Temperature (ºC)							Extruder Speed (rpm)
Zone I	Zone II	Zone III	Zone IV	Zone V	Zone VI	Nozzle	
145	145	150	150	145	140	135	150

296

297 After obtaining the granules of PLA (control) and biocomposites, the necessary
298 specimens were manufactured for each of the materials by injection moulding to carry
299 out the different characterisation tests. Before the injection moulding process, moisture
300 was removed from the materials in a KKT 75 dryer (KOCH, Germany) under the
301 following conditions: 45 ºC for 5 h. The equipment used to carry out the injection
302 moulding process was an ENGEL Victory 28 machine (Engel Holding GmbH, Austria)
303 and the specimens obtained were those whose dimensions comply with ISO 527-2 and
304 179-1 standards, respectively [35] [36].

305 *2.6. Characterisation of PLA and polymer biocomposites*

306 *2.6.1. Mechanical properties*

307 Tensile properties were determined according to ISO 527-2 standard using a "Tinius
308 Olsen 10KS" universal testing machine and 75 mm long and 2 mm thick haltere 1BA
309 type specimens [35]. A Charpy Impact Meter Izod IMPats 2281 (Metrotec, Spain) was
310 used to determine Charpy impact strength of the different materials according to ISO 179-
311 1 standard using 80 mm·10 mm·4 mm specimens [36].

312 *2.6.2. Structural and morphological analysis*

313 The composition of the biocomposites was determined by XRD in an Empyrean
314 equipment with a PIXcel-3D detector from PANalytical (Malvern PANalytical, United
315 Kingdom) and they were recorded in the 2θ range from 10 to 60º with a step size of 0.02.
316 The most interesting chemical bonds to understand the structure of the materials were
317 determined using ATR-FTIR Vertex 70 (Bruker, United States). Scans were performed
318 in the 4000-400 cm-1 frequency range. The SEM images of the raw PLA and the different
319 mechanically tested biocomposites were obtained using the same equipment and
320 methodology previously described in section "2.4.3. Scanning Electron Microscopy" with
321 the difference that the samples did not require prior drying. and an accelerating voltage
322 of 15 kV was used.

323 *2.6.3. Thermal properties*

324 Thermal behaviour of the materials was determined in a Differential Scanning
325 Calorimetry (DSC) 822e Mettler Toledo equipment (Mettler-Toledo, Switzerland). The
326 temperature ramps were 5 ºC/min, in heating mode in the range of 30 to 200 ºC, a
327 temperature at which it was maintained for about three hours, followed by subsequent
328 cooling to 30 ºC. After performing the DSC analysis, the values of the crystallisation
329 temperature (T_c) and the melting temperature (T_m) were obtained from a maximum and a
330 minimum point respectively of each of the resulting DSC curves. The percentage of
331 crystallinity was calculated using Equation 8:

332 $$W_c\,(\%) = \frac{\Delta H_m}{\Delta H_{mc}} \cdot \frac{1}{f_{PLA}} \cdot 100 \qquad \text{Eq. (8)}$$

333 Being ΔH_m (J/g) the melting enthalpy of the analysed material calculated as the area on
334 the curve where the minimum point corresponding to T_m is located, ΔH_{mc} (J/g) the melting
335 enthalpy corresponding to the 100% crystalline PLA sample (93.7 J/g) [37] and f_{PLA} the

weight fraction of PLA in the biocomposite. The enthalpy of crystallization (ΔH_c) was also determined, specifically as the area under the curve where the maximum point corresponding to T_c is located.

The thermal stability of the different materials (raw PLA and biocomposites) was determined using the same equipment and the same procedure described in section "2.4.6. Thermogravimetric Analysis (TGA)" with the only difference being that the maximum temperature reached in the experiment was 900 ºC. The aim of these tests is to obtain the temperature at which thermal degradation of the material begins ($T_{d,i}$), temperature at which the maximum in the area of the DTG curve corresponding to the thermal degradation of the material is reached ($T_{d,max}$), temperature at which complete degradation of the material ends ($T_{d,f}$) and percentage of solid residue (ash) remaining after analysis.

2.6.4. Water absorption

The water absorption capacity of the raw PLA and the different biocomposites was determined according to a procedure based on method 2 of the ISO 62 standard [38] and using 80 $mm^{\cdot 10}$ $mm^{\cdot 4}$ mm test tubes manufactured by injection moulding. Specifically, applying the indicated methodology, the percentage change in mass, c(%), relative to the initial mass was determined before using Equation 9:

$$c(\%) = \frac{m_2 - m_1}{m_1} \cdot 100 \qquad \text{Eq. (9)}$$

Being m_1 is the mass in mg of the test piece after initial drying and before immersion in water; and m_2 the mass in mg of the specimen after immersion in water.

3. Results and discussion

3.1. Chemical composition of OTP biomass

The examination of the chemical composition of the untreated biomass is essential in order to develop an efficient methodology able to achieve the targeted goals, in this case the removal of non-cellulosic compounds and the isolation of the cellulose fraction. The analysis performed showed that untreated OTP contained 7 wt.% moisture, and 0.178 wt.% ash. In addition, the cellulose, hemicellulose and lignin contents were 31.53 wt.%, 21.61 wt.% and 24.76 wt.% respectively, which are within the ranges normally found for woody biomass [39]. Regarding the cellulose content of OTP biomass, of great interest for this work, other authors have reported values oscillating between 22.30 wt.% and 41.41 wt.% [5][40][41][42]. This variability may be ascribed to the differences derived from the analytical methodology followed for the determination of the chemical composition of OTP [39].

3.2. Isolation of cellulose from OTP biomass

3.2.1. Optimisation of the acid hydrolysis process

Depending on the treatment performed, yellowish-brown OTP fibres were obtained after hydrolysis with HNO_3. The percentages hydrolysed of cellulose (Y_{cell}), hemicellulose (Y_{hemi}) and lignin (Y_{lig}), as well as the $Yield_{AH}$ and the *CrI* values of OTP biomass after hydrolysis with HNO_3 at the conditions described in the DOE are depicted in Table 1. As observed, the $Yield_{AH}$ varied in the range 30.90-80.23% coinciding the limits with the harsher (AH_8) and milder (AH_1) hydrolysis conditions. Kian et al. (2020) have recently obtained a reaction yield of 47.6% by extracting OTP fibres by a conventional two-step sodium chlorite bleaching and soda pulping process [5].

The results in Table 1 were used for statistical analysis and to predict the quadratic regression equations of the response functions after eliminating non-significant coefficients, and replacing coded variables by real values (Eqs. (10-13)).

382 $$Y_{cell} = 38.99 + 1.79t + 4.15T + 4.54c - 3.83T^2 - 4.37Tc - 1.26tc$$ Eq. (10)

383 $$Y_{hemi} = 65.68 + 2.28t + 17.93T + 10.63c - 3.92T^2 - 2.71Tc$$ Eq. (11)

384 $$Y_{lig} = 64.49 + 6.21t + 15.53T + 22.49c - 5.81T^2 - 8.34c^2$$

385 $$+5.29Tt - 5.42tc$$ Eq. (12)

386 $$CrI = 52.84 + 0.10t + 5.33T + 4.49c + 0.83t^2 + 0.91Tt$$ Eq. (13)

Table 1. Matrix of the experimental design performed for the AH process (coded values of the independent variables in brackets) and results obtained for the response variables

TREATMENT	t, min	T, ˚C	c, % w/v	Y_{cell}, %	Y_{hemi}, %	Y_{lig}, %	CrI, %	$Yield_{AH}$, %
AH_1	120(-1)	60(-1)	2(-1)	19.29	29.48	10.88	44.39	80.23
AH_2	240(1)	60(-1)	2(-1)	25.19	33.35	17.33	42.50	74.86
AH_3	120(-1)	90(1)	2(-1)	37.00	71.19	18.34	53.46	57.01
AH_4	240(1)	90(1)	2(-1)	41.49	71.47	59.38	55.28	45.41
AH_5	120(-1)	60(-1)	8(1)	38.67	57.94	58.46	53.99	53.44
AH_6	240(1)	60(-1)	8(1)	39.45	56.26	56.64	51.69	55.97
AH_7	120(-1)	90(1)	8(1)	38.83	85.03	84.41	62.67	31.89
AH_8	240(1)	90(1)	8(1)	38.37	87.33	90.36	63.92	30.90
AH_9	95.4(-1.41)	75(0)	5(0)	35.57	54.77	53.10	54.03	58.99
AH_{10}	264.6(1.41)	75(0)	5(0)	43.20	70.79	69.26	55.68	47.50
AH_{11}	180(0)	53.85(-1.41)	5(0)	26.26	31.20	27.46	45.84	77.67
AH_{12}	180(0)	96.15(1.41)	5(0)	38.03	85.62	81.93	60.79	35.28
AH_{13}	180(0)	75(0)	0.77(-1.41)	30.62	48.95	19.37	46.68	76.58
AH_{14}	180(0)	75(0)	9.23(1.41)	46.25	81.72	79.96	58.82	39.69
AH_{15}	180(0)	75(0)	5(0)	40.29	68.12	65.96	53.46	57.50
AH_{16}	180(0)	75(0)	5(0)	38.96	68.27	67.39	53.67	47.52
AH_{17}	180(0)	75(0)	5(0)	39.62	68.20	66.68	51.38	51.43

Independent variables t, T and c correspond to reaction time (min), reaction temperature (˚C) and HNO_3 concentration (% w/v). Y_{cell}, Y_{hemi} and Y_{lig} are the concentration of cellulose, hemicellulose and lignin in the hydrolysates; CrI is the crystallinity index; and $Yield_{AH}$ is the yield of each AH reaction.

Figure 1 presents the representation of the values obtained from the DOE against those predicted for the quadratic equations for each response variable considered.

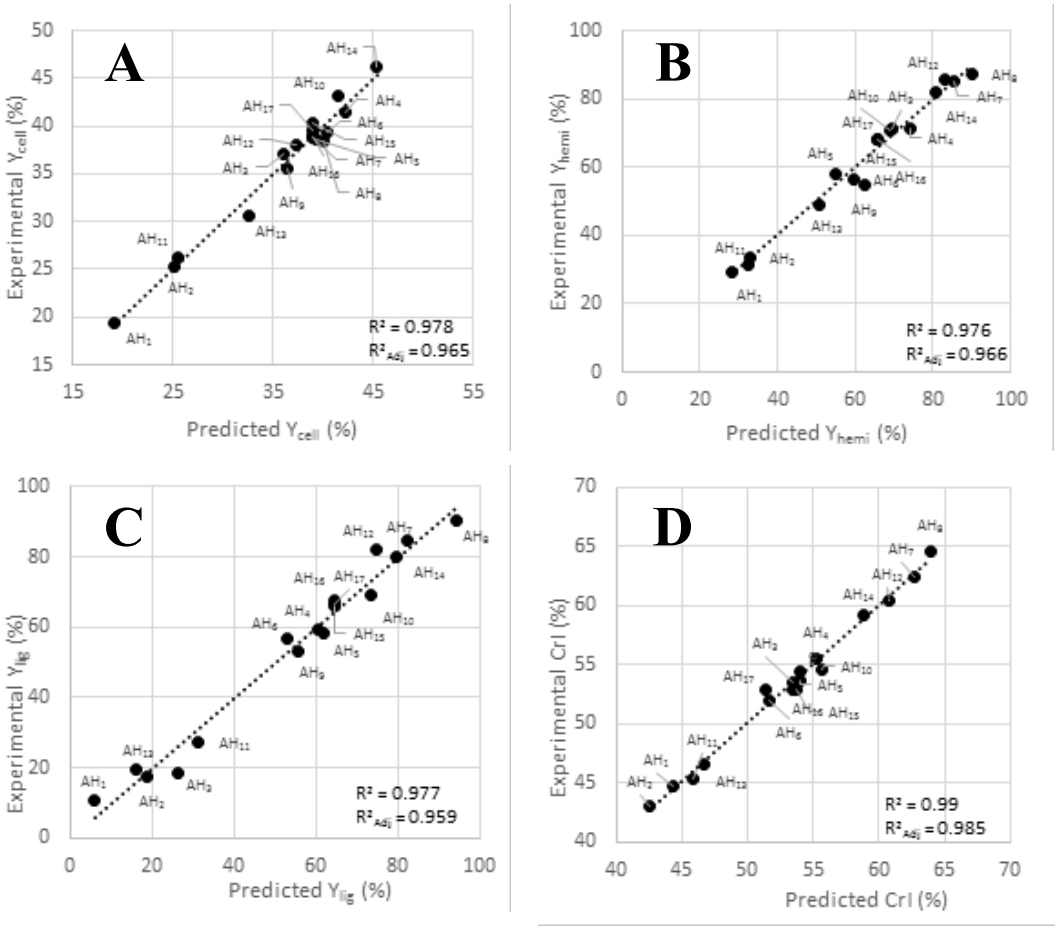

Figure 1. Experimental results versus those predicted by the models for Y_{cell} (A), Y_{hemi} (B), Y_{lig} (C) and CrI (D).

As observed, the statistical significance of the model is confirmed by the high values of the determination coefficients ($R^2 \geq 0.976$) and adjusted determination coefficients ($R^2_{adj} \geq 0.959$). This indicates that the quadratic regression equation models of the response variables have good statistical validation for the prediction of experiments within the conditions used in this study [43][44][45].

The effect of the independent variables on the response functions are shown by the linear, quadratic and interactive coefficients of the regression equations, and by the RSM plots that were constructed with varying *t* and *T* values, and retaining the variable *c* at the three levels tested (Figure 2).

406

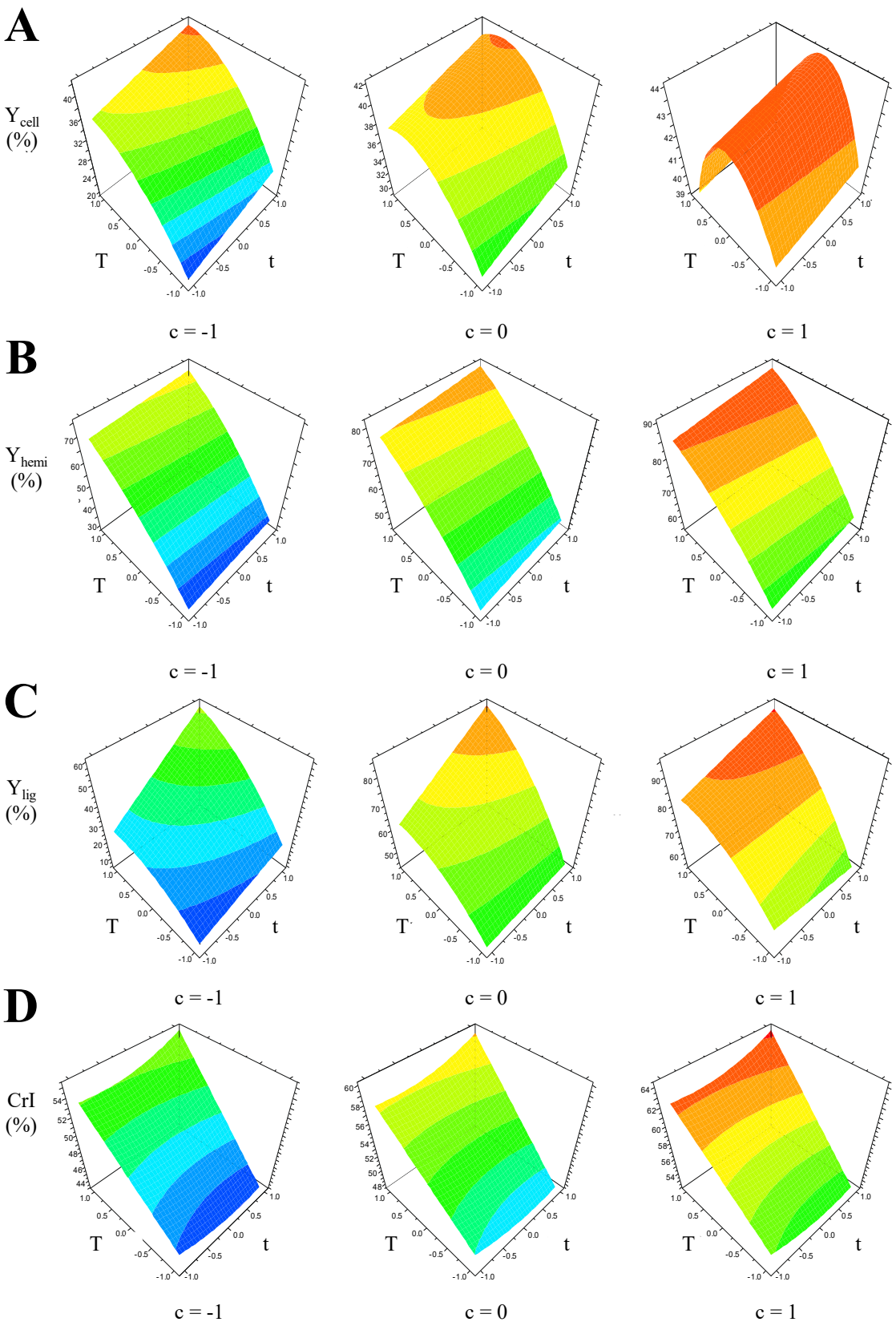

407
408 **Figure 2.** Response surfaces from the experimental design showing the interactive effect of *t*, *T*
409 and *c* on Y_{cell} (A), Y_{hemi} (B), Y_{lig} (C) and *CrI* (D).

These RSM curves identified the optimum conditions for the maximum Y_{hemi} and Y_{lig}, while maintaining a relatively low cellulose removal. Y_{cell} oscillated between 19.29% for AH_1 run, using milder conditions, and 46.25% for AH_{14} assay, which consisted of the highest HNO_3 concentration and intermediate *t* and *T*. On the other hand, the maximum values of Y_{hemi} and Y_{lig} were 87.33% and 90.36 % respectively, both obtained for run AH_8 with *c* 8%, *T* 90 °C and *t* 240 min.

As expected, the increase of either *t*, *T* or *c* led to an enhanced Y_{cell}, Y_{hemi} and Y_{lig} (Eqs. (10-12); Figures 2A-C). It is remarkable the higher values of these coefficients for Y_{hemi} and Y_{lig}, especially for *T* and *c*, and the lower effect of *t*, thus confirming that the time of reaction had less influence on the hydrolysis of the lignocellulosic biomass [46]. Moreover, although hemicellulose and lignin were more easily hydrolysed, the cellulose chains were also attacked by HNO_3 at different extent depending on the conditions used (Table 1). On the other hand, the quadratic term T^2 produced a significant decrease in the hydrolysis of the three components (Eqs. (10-12)), which was more pronounced for Y_{cell} particularly at the highest HNO_3 concentration (Figure 2B). In addition, the negative value of the coefficient c^2 indicated a decreasing effect on Y_{lig} (Eq. (12)). However, the effect of t^2 on Y_{cell}, Y_{hemi} and Y_{lig} was not significant.

The affecting variables on *CrI* were the three linear terms, the quadratic coefficient t^2 and the interactive *Tt* (Eq. (13)). All of these coefficients showed a positive influence on *CrI*, especially *T* and *c*, which is in agreement with the removal of hemicellulose and lignin from OTP biomass. Again, the influence of *t* on the CrI values of the hydrolysed OTP fibres was practically negligible (Figure 2D).

From these results and despite that $Yield_{AH}$ was low (Table 1), AH_8 treatment was selected as optimum to maximise Y_{hemi} and Y_{lig}, thus obtaining an OTP sample enriched in cellulose OTP fibres after AH_8 treatment contained 63.32 wt.% cellulose, 8.92 wt.% hemicellulose,

435 and 7.78 wt.% lignin. By substitution of the specific experimental conditions of AH_8 (t =
436 1; T = 1; c = 1) in the regression equations, Y_{cell}, Y_{hemi}, Y_{lig} and CrI values of 40.01%,
437 89.89%, 94.44% and 64.50% respectively were obtained, which are slightly higher than
438 those from the experiment. More particularly predicted values of Y_{cell}, Y_{hemi}, Y_{lig} and CrI
439 were 4%, 3%, 5% and 1% higher. These slight differences again verified the good fitting
440 of the regression models with the experiments.

441 *3.2.2. Alkaline hydrolysis*

442 Once the AH conditions were optimised, the resulting solid from AH_8 experiment was
443 further purified by two different hydrolysis reactions with diluted NaOH at the
444 experimental conditions described in section 2.4.2. Treatment with NaOH at different
445 experimental conditions is frequently referred in literature as the first hydrolysis step for
446 the isolation of cellulose from lignocellulosic biomass [31][32][42][43].

447 A yield of 82.75% was obtained for BH_1 treatment, whereas $Yield_{BH2}$ was slightly lower
448 (74.11%) due to the harsher conditions followed in BH_2. Because of this, BH_2 treatment
449 achieved greater hydrolysis rates of both hemicellulose and lignin, and the resulting OTP
450 fibres contained a higher amount of cellulose by comparison with BH_1 (Table 4).

451 **Table 4.** Yield of BH treatments and chemical composition of the OTP fibres obtained

TREATMENT	Cellulose (wt.%)	Hemicellulose (wt.%)	Lignin (wt.%)	$Yield_{BH}$ (%)
BH_1	71.91	6.92	6.98	82.75
BH_2	83.28	0.50	5.00	74.11

452 The content of cellulose after the BH_2 reaction amounted to over 80 wt.%, whereas that
453 of lignin and especially hemicellulose can be considered negligible. Similarly, other
454 authors have recently reported 79.8 wt.% cellulose in OTP fibres after a bleaching-
455 alkaline hydrolysis procedure [5]. In contrast, Sánchez-Gutiérrez et al. (2020) obtained a
456 cellulose content of 59.7 wt.% from OTP biomass after a soda pulping process with a

yield of 32%. As expected, the cellulose content of OTP fibres increased after the chemical treatments from 31.53 wt.% in the raw OTP to 83.28 wt.% after both hydrolysis reactions [42]. In addition, the procedure followed was highly efficient in hydrolysing hemicellulose and lignin, which decreased from 21.61 wt.% to 0.50 wt.% and from 24.76 to 5.00 wt.% respectively. Therefore, the combination of AH_8 and BH_2 hydrolysis reactions in this study may be established as an appropriate method in order to isolate pulp rich in cellulose from OTP biomass. This purification is reflected by the change of colour of OTP after the consecutive AH_8 and BH_2 treatments (Figure 3).

3.3. Characterisation of OTP biomass at each stage of treatment

3.3.1. Scanning Electron Microscopy

The chemical treatments also induced structural and morphological changes in OTP fibres at the microscopic level. Figure 3A shows that OTP presents a compact surface with a somewhat rough texture formed by strongly bonded fibres, typical of lignocellulosic biomass [31][32][33]. The AH_8 treatment involves a loss of the most superficial layers of the OTP fibres and an increase in the surface roughness by separating the bundles of fibres (Figure 3B). This is related to the partial elimination of non-cellulosic components such as lignin, hemicellulose, pectin and waxes from outer layers. Finally, BH_2 reaction led to an additional removal of non-cellulosic compounds, thus causing the swelling of the fibre bundles and their almost total separation into individual fibres of smaller diameter (Figure 3C). This swelling process facilitates the disintegration of the fibres into a smooth-surfaced fibrillary structure, indicative of greater removal of impurities [47]. This agrees with the results obtained in the previous chemical characterisations that revealed a small amount of hemicellulose and lignin remaining in the solid.

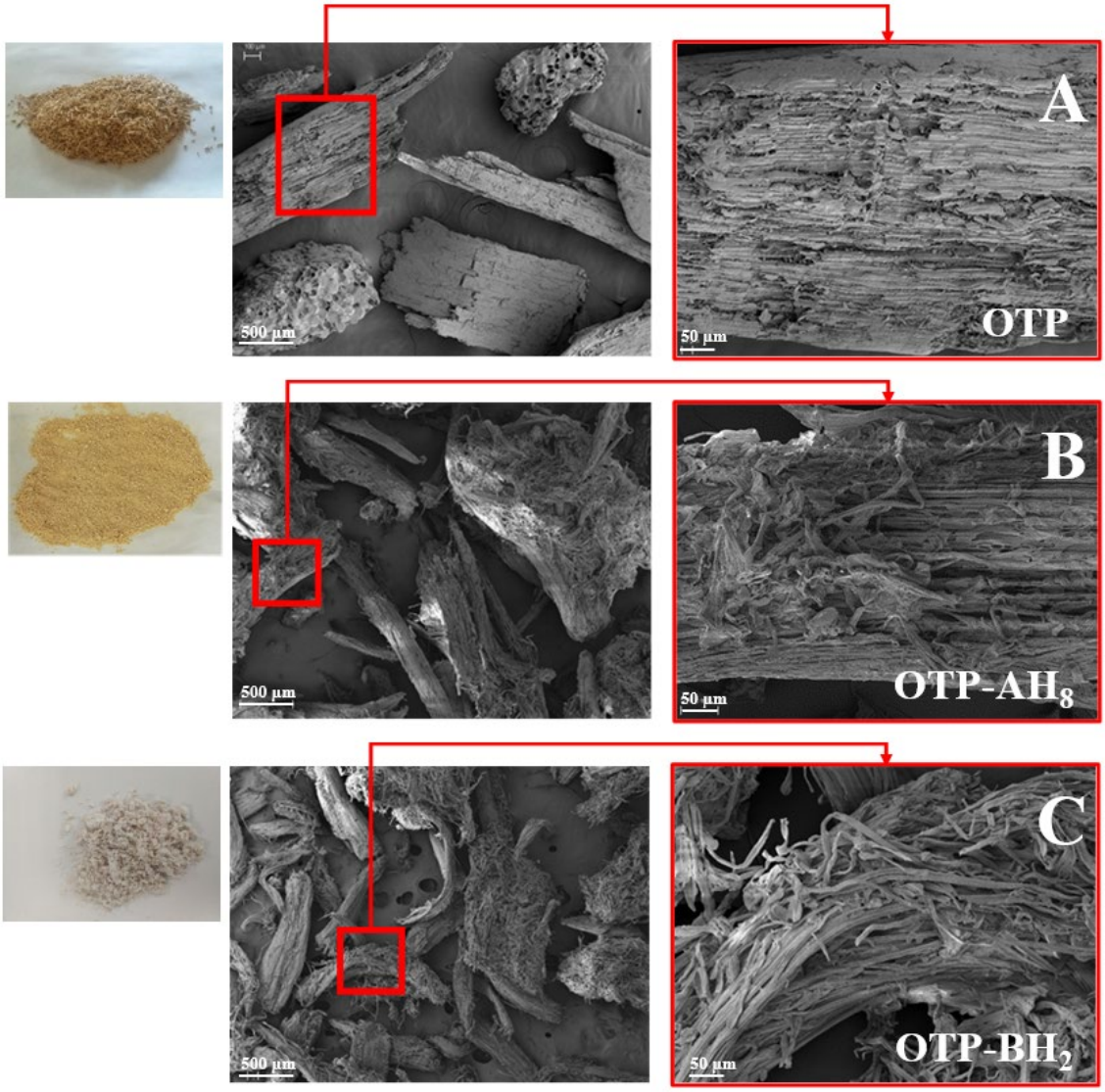

Figure 3. Scanning electron micrographs of untreated OTP fibres (A), AH_8-treated fibres (B), and BH_2-treated fibres (C).

3.3.2. Fourier-Transformed Infrared Spectroscopy

The characterisation of OTP, OTP-AH_8 and OTP-BH_2 fibres by means of FTIR spectroscopy allowed to determine the influence of the selected acid and alkaline treatments on the chemical structure of OTP. Figure 4 shows the FTIR spectra of the different OTP biomass samples, in which the main characteristic bands of cellulose, lignin and hemicellulose were easily identified. In addition, the chemical treatments led to changes in the intensity of the bands, which indicates changes in the composition of the fibres. The broad band at 3000-3700 cm^{-1}, corresponding to the stretching vibration of –

OH bonds in cellulose, hemicellulose and lignin, reflects the hydrophilic character of the fibres [32][48]. When comparing the spectra, it is observed that the area under the band at 3100–3700 cm^{-1} was intensified after the AH_8 reaction, indicating that the fibres reacted with the acid. As a consequence, there was an increase in the percentage of hydroxyl groups, this effect being even greater after the alkaline treatment. The peak observed in the region 2800-2900 cm^{-1} is ascribed to the C−H stretching in the functional groups – CH_2 and –CH_3 of lignin and cellulose [32]. The bands at 1600-1740 cm^{-1} are attributed to the stretching of C=O bonds in acetyl and uranic-esther groups in hemicellulose, and to the ferulic and *p*-coumaric acids in the lignin structure [48][49]. Because of this, the absorption in this region is less intense in the spectra of OTP-AH_8 and OTP-BH_2 samples, with lower contents of hemicellulose and lignin. As the samples were subjected to the successive stages of the global chemical treatment, an increase in their hydrophilic character was observed. This is determined by the increase in the size of the band associated with the moisture absorption of the fibres, more specifically that located between 1635-1650 cm^{-1} [12].

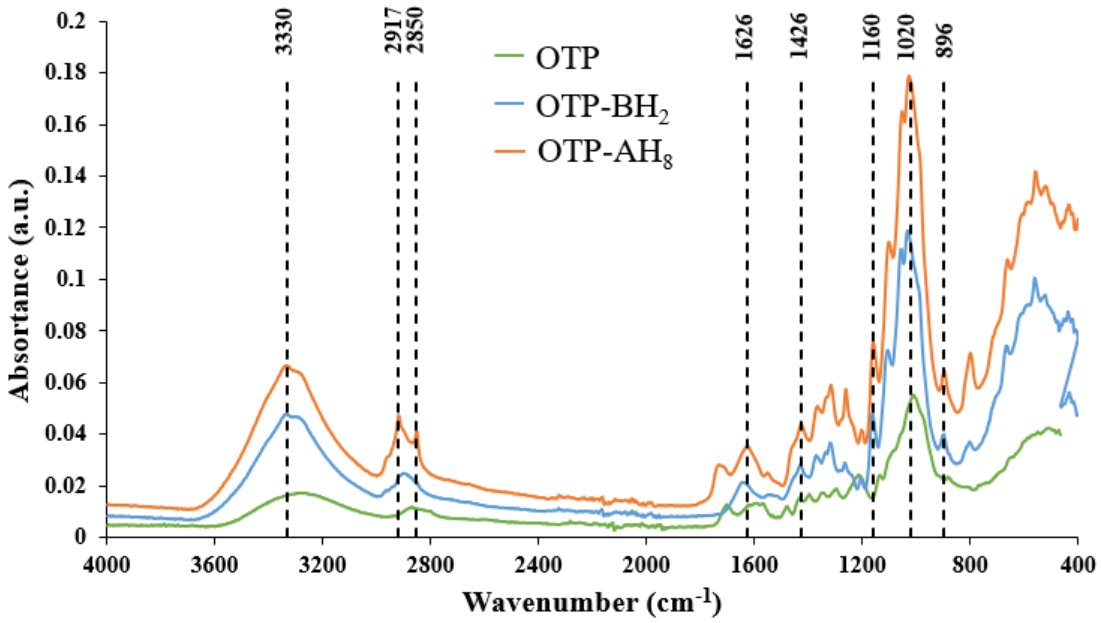

Figure 4. FTIR spectra of untreated OTP fibres, AH_8-treated fibres, and BH_2-treated fibres.

A similar effect is observed in the region 1400-1550 cm^{-1}, which is related to the stretching vibration of the C=C bonds in the aromatic backbone of lignin [48]. The bands at wavenumbers 1240-1160 cm^{-1} have been related to the vibration of the C–O bond of the acetyl groups present in lignin, and to the stretching and deformation of the C−O bond in cellulose and hemicellulose [49]. This band is very well defined in OTP fibres but, as above, the intensity of the spectra at this region is decreased in both OTP-AH_8 and OTP-BH_2 fibres. This phenomenon indicates that non-cellulosic components initially present in the OPT biomass were partially eliminated with the treatments. Finally, the peaks observed in the region of approximately 1100-1020 cm^{-1} are associated to the C−O−C vibration of glycosidic ethers, and to the glycosidic links between monosaccharides in the cellulose skeleton. The appearance of this band in both original and treated biomass confirmed that the chemical treatments did not change the cellulose structure [33]. Furthermore, the peak at approximately 890 cm^{-1} is also related to β-glycosidic bonds between glucose molecules in the cellulose chains [32].

It can be said from these results that there were no significant variations between the spectra in terms of the location of the main peaks, but significant changes in their intensity were found. It indicates that hemicellulose, lignin and other impurities on the fibre surface were partially removed as a result of the treatments, without introducing new chemical functionalities.

3.3.3. X-Ray Diffraction

Cellulose has a semi-crystalline structure represented by cellulose I crystalline domains with adjacent H-bonded chains embedded in an amorphous matrix [50]. The crystalline structure of the different OTP samples was investigated by XRD. XRD patterns of OTP, OTP-AH_8 and OTP-BH_2 showed 3 peaks typical of cellulose I at 2θ values of approximately 16° (corresponding to the (110) reflection plane), 22.5° (attributed to the

(200) lattice plane of cellulose sheets), and 34.5° (sensitive to the alignment of chains into the fibrils) (Figure 5) [3]. The similarity of the diffractograms indicates that the polymorphism of cellulose I is maintained after the hydrolysis treatments [32]. On the other hand, the intensity of the peaks is higher for the fibres after chemical treatments, especially for the fully hydrolysed OTP-BH_2 sample. This is consistent with the *CrI* values, which varied from 40.92% for OTP to 71.06% for OTP-BH_2 in accordance with the progressive elimination of amorphous components with the treatments [33]. A recent study found *CrI* 60.26% for NaOH-OTP pulp [33], and in the range 74.8-83.1% for cellulose nanocrystals synthesized from OTP biomass [5]. Moreover, the cellulose *CrI* reported in this work is comparable with those for other lignocellulosic biomasses from varied sources [6][32][43][51].

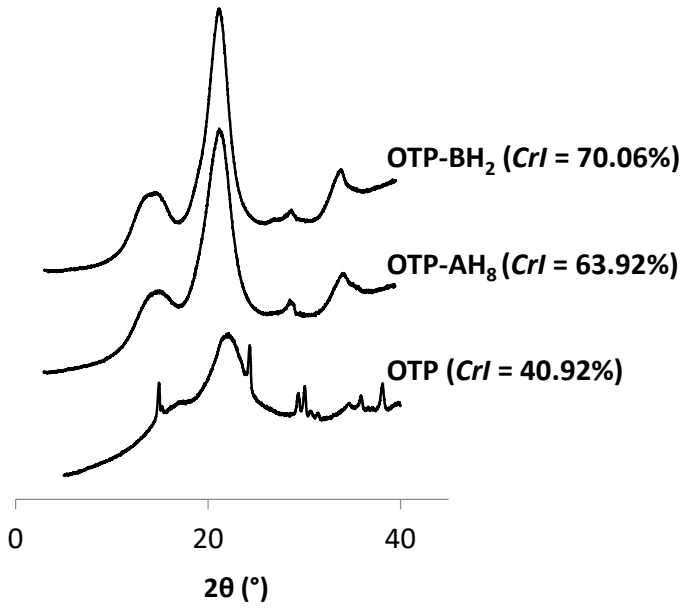

Figure 5. X-Ray Diffractograms of untreated OTP fibres (bottom), OTP-AH_8 fibres (middle), and OTP-BH_2 fibres (top), and their respective crystallinity indexes (*CrI*).

3.3.4. Thermogravimetric Analysis

TGA was performed to evaluate the thermal stability of OTP biomass at each stage of treatment. The initial weight loss below 100 °C in Figure 6 is related to the evaporation

of volatile compounds, and water retained in the fibres. This peak is more visible for untreated OTP due to its stronger hydrophilic character. Subsequently, degradation of cellulose, hemicellulose and lignin occurred between approximately 200 and 400 °C. In the case of raw OTP fibres, this event appears as a broad band due to its higher content of hemicellulose, lignin and other non-cellulosic compounds. As reported by some studies [32][50], the degradation of hemicellulose and lignin may be masked by the main degradation peak of cellulose. Therefore, this peak became narrower as the chemical treatment of the fibre progressed.

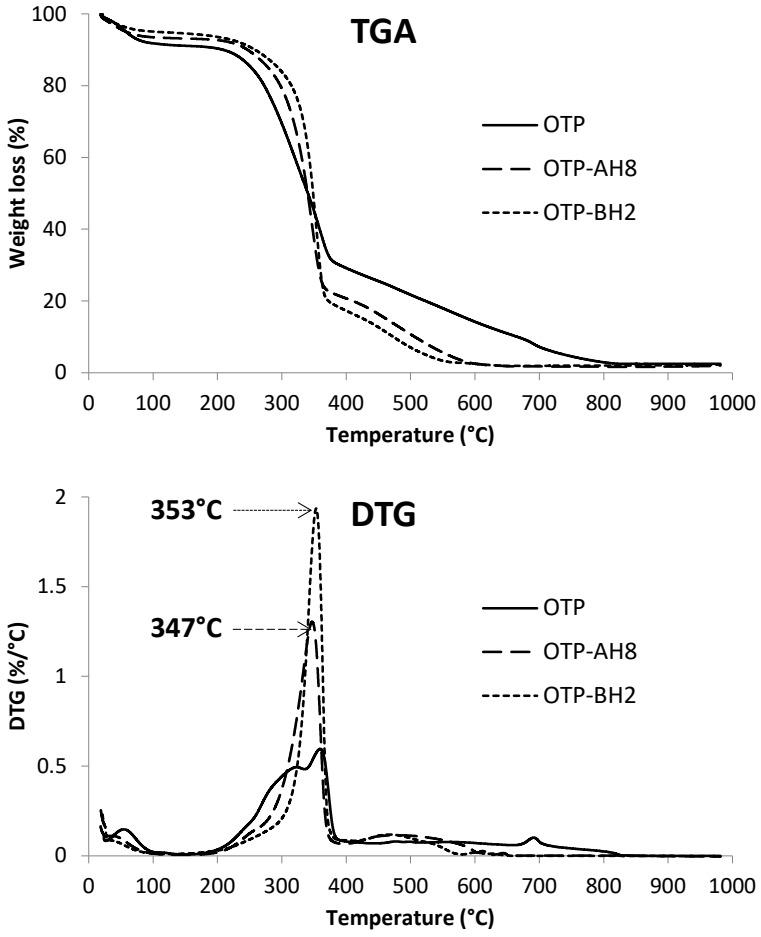

Figure 6. TGA and DTG curves of untreated OTP fibres, OTP-AH_8 fibres, and OTP-BH_2 fibres.

As observed in the DTG curves, the three samples presented a T_{onset} temperature around 200 °C. However, the maximum degradation temperature (T_{max}) was dependent on the chemical composition of the fibres. OTP did not present a defined value, whereas T_{max}

568 for OTP-AH_8 and OTP-BH_2 was 347 °C and 353 °C respectively (Figure 6). This is
569 consistent with the progressive elimination of non-cellulosic components with lower
570 thermal stability than cellulose [12][31][32][33][48], and agrees with previous results
571 observed in FTIR and XRD. Our findings coincide with that from Sánchez-Gutiérrez et
572 al. (2020) who reported a T_{max} of 348 °C for a cellulosic pulp extracted from OTP biomass
573 with 16% NaOH at 170 °C [42]. Finally, it is also remarkable to mention the higher
574 residue amount of unhydrolysed OTP, which has been associated with a higher carbon
575 content in the fibres and with the presence of ash and lignin [31][33].

576 *3.4. Characterisation of PLA and bicomposites*

577 *3.4.1. Mechanical properties*

578 Figure 7 shows the value of those parameters obtained from the tensile and impact tests:
579 tensile strength, elongation at break, Young's modulus and impact strength. Tensile
580 strength (Figure 7-A) increased with the addition of 5 wt.% OTPBH_2 by 9.4%, however
581 when 15 wt.% OTPBH_2 was reached, it is reduced by 37.7%. The reduction in the tensile
582 strength value when the OTPBH_2 content increases in the biocomposite is mainly due to
583 the fact that a higher percentage of the load induces the self-aggregation of the cellulose
584 particles, due to the formation of hydrogen bonds [52]. Elongation at break (Figure 7-B)
585 also decreased with the addition of OTPBH_2. When it comes to OTP as filler, tensile
586 strength remains below that of pure PLA. The reduction in the tensile strength and the
587 elongation at break with increasing fibre content may be due to the reduction in L/D ratio
588 in the cellulose fibres. The reduction of the L/D ratio occurs because a high content of
589 this filler generally causes a mechanical breakage of the fibres due to the friction that
590 takes place between the fibres themselves, which in turn ultimately leads to a poor stress
591 transfer from the fibre to the matrix [53]. Young's Modulus (Figure 7-C) decreased with
592 the incorporation of 5 wt.% OTPBH_2, and increased when 15 wt.% was reached.

593 However, in the case of those samples with OTP, there was no increase in Young's
594 Modulus. Therefore, the improvement in terms of mechanical properties by removing
595 hemicellulose and lignin from the lignocellulosic fibres was due to a better interaction
596 between the fibre and the polymer matrix, as reported by other authors [54]. The presence
597 of cellulose fibres restricted the mobility of PLA polymer chains, reducing free volume,
598 resulting in poor stress transfer and resulting in increased stiffness in biocomposites [19].
599 The impact strength (Figure 7-D) of the biocomposite decreased with the presence of OTP
600 and $OTPBH_2$, this decrease being more significant when the load percentage increased.
601 This is due to the presence of stress concentrators at the fibre-matrix interface, which
602 promotes the initiation of the fracture [55]. Reinforcement with fibres with a higher
603 cellulose content improves impact strength of biocomposites compared to untreated OTP
604 fibres. This improvement is greater for 15 wt.% of reinforcement, being 67% with respect
605 to the OTP. In addition, the impact resistance value is maintained by increasing the
606 percentage of reinforcement with $OTPBH_2$.

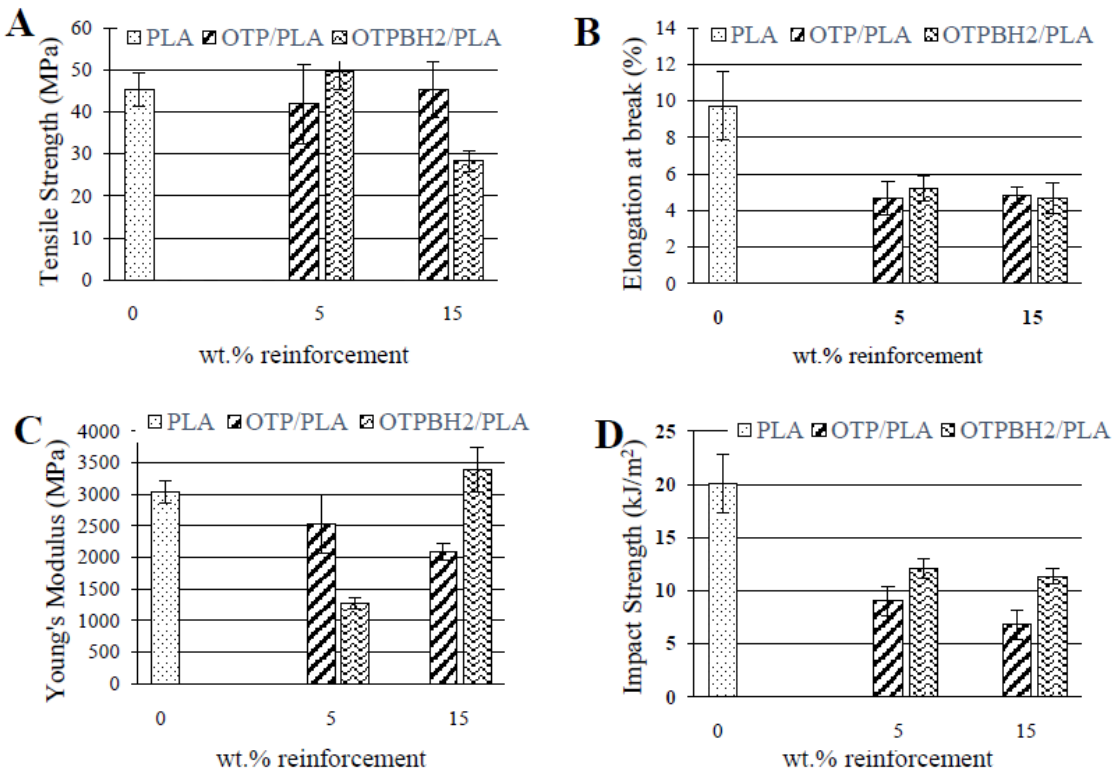

607

Figure 7. Mechanical properties of PLA and biocomposites: (A) Tensile Strength; (B) Elongation at break; (C) Young's Modulus; (D) Impact Strength.

3.4.2. Structural and morphological analysis

Figure 8 shows the FT-IR spectra of the PLA and the PLA-based biocomposites. The main peaks attributed to PLA matrix are identified at 2910 and 1717 cm^{-1}, corresponding to the -CH and C=O groups, respectively [56]. Those bands attributed to the vibration of the -CO groups, located at 1160, 1108 and 1063 cm−1, were also identified [57]. The spectrum of all the biocomposites shows a similar trend in terms of the position of the peaks. However, there is a broadening in the region of 3000-3600 cm-1 associated with the presence of -OH groups. There is also a variation of the intensity of the peaks, which demonstrates that the incorporation of the fibres does not generate a substantial change in the chemical composition of the developed biocomposites [58].

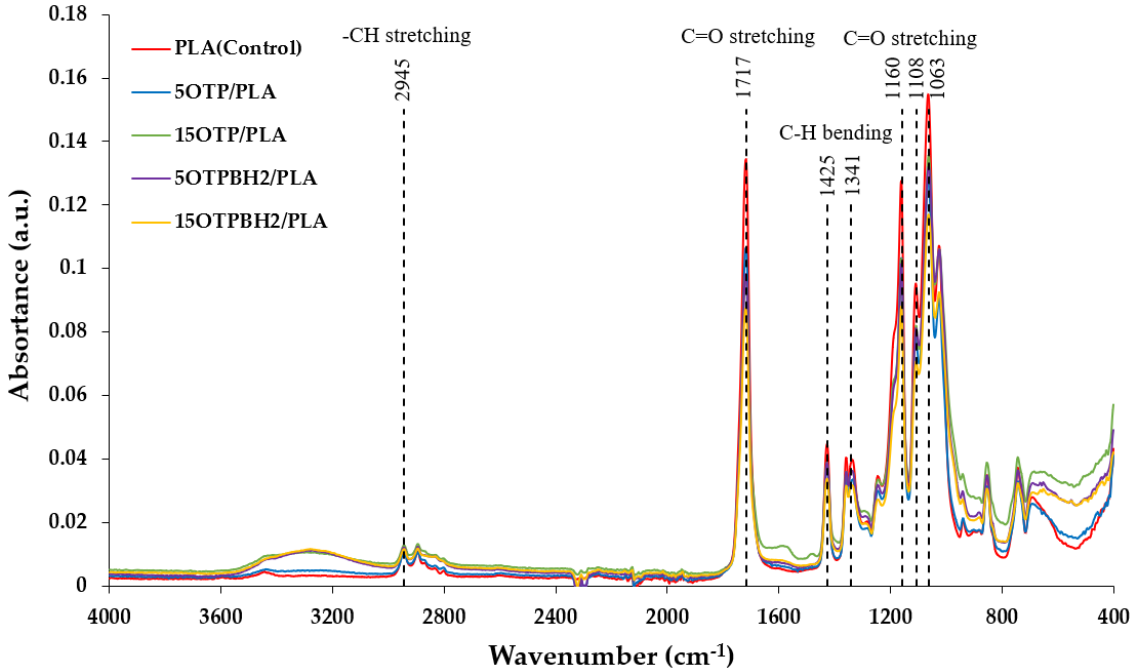

Figure 8. FT-IR spectra of biocomposites.

The XRD patterns obtained are shown in Figure 9.

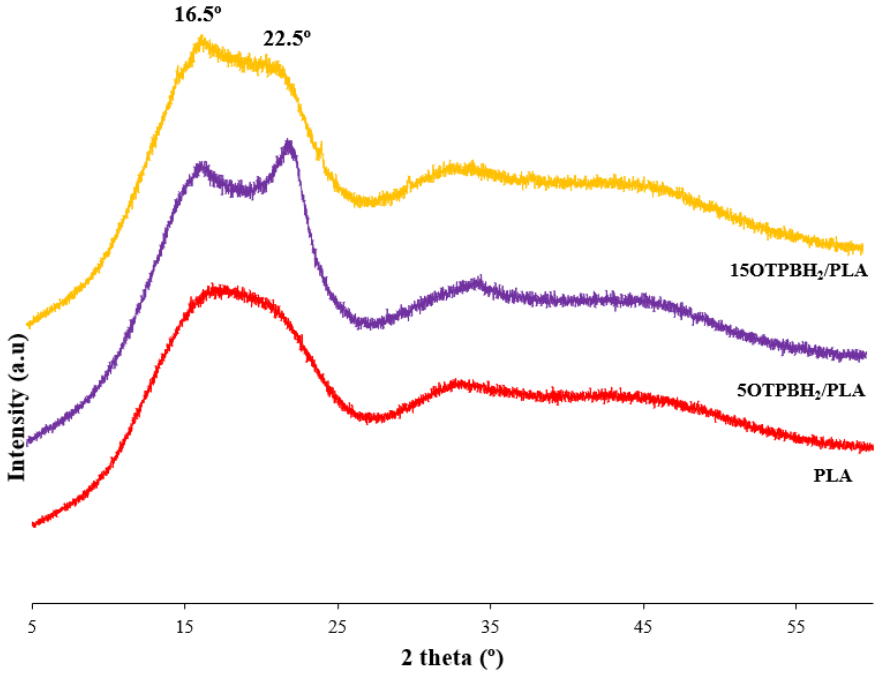

Figure 9. XRD of biocomposites.

XRD pattern for PLA revealed a wide hump for 2θ values around 16.4°, without a discernible crystalline peak, which can be associated with the crystallographic plane [211]/[110], typical of a semi-crystalline polymer [19][59]. In the spectra of those samples containing $OTPBH_2$, the appearance of two main peaks located at 16.5° and 22.5° was observed, which is indicative of the presence of type I cellulose, indicative of a polymorphic structure in the biocomposites [48].

The morphology of the fracture surfaces resulting from the Charpy impact resistance tests carried out on the materials are shown in Figure 10. Both the OTP and $OTPBH_2$ reinforcement are covered by layers of the PLA matrix, however, those materials manufactured with untreated fibre presents a less continuous fracture surface, a greater number of voids (Figures 10B and 10D) and worse adhesion between fibre and matrix than in the case of those materials made with chemically treated fibre [60].

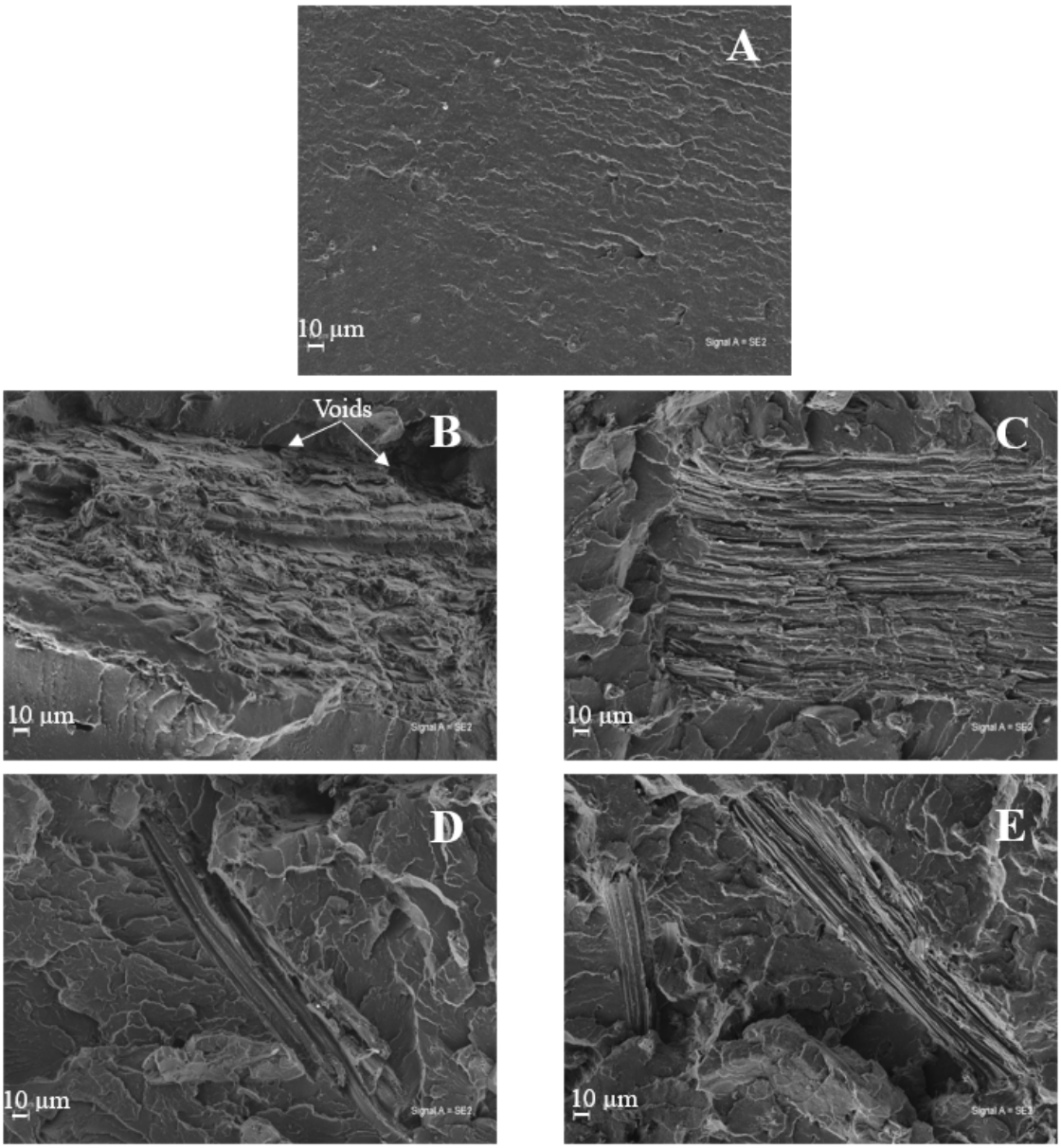

640 **Figure 10.** SEM of biocomposites: (A) PLA(Control); (B) 5OTP/PLA; (C)5OTPBH$_2$/PLA; (D)
641 15OTP/PLA; (E)15OTPBH$_2$/PLA.
642

643 *3.4.3. Thermal properties*

644 The thermal properties obtained from the DSC curves of PLA and the fabricated
645 biocomposites (Figure 11) are shown in Table 5.

646 **Table 5.** Thermal properties obtained from PLA and biocomposites DSC curves

Material Reference	T_c (ºC)	T_m (ºC)	ΔH_m (J/g)	ΔH_c (J/g)	W_c (%)
PLA (Control)	94.63	172.00	35.48	21.08	38.44
5OTP/PLA	-	171.96	47.73	-	54.48
5OTPBH$_2$/PLA	92.74	171.05	35.43	20.45	40.44

15OTP/PLA	92.05	173.54	34.67	16.77	44.32
15OTPBH$_2$/PLA	92.08	171.00	30.68	18.59	39.21

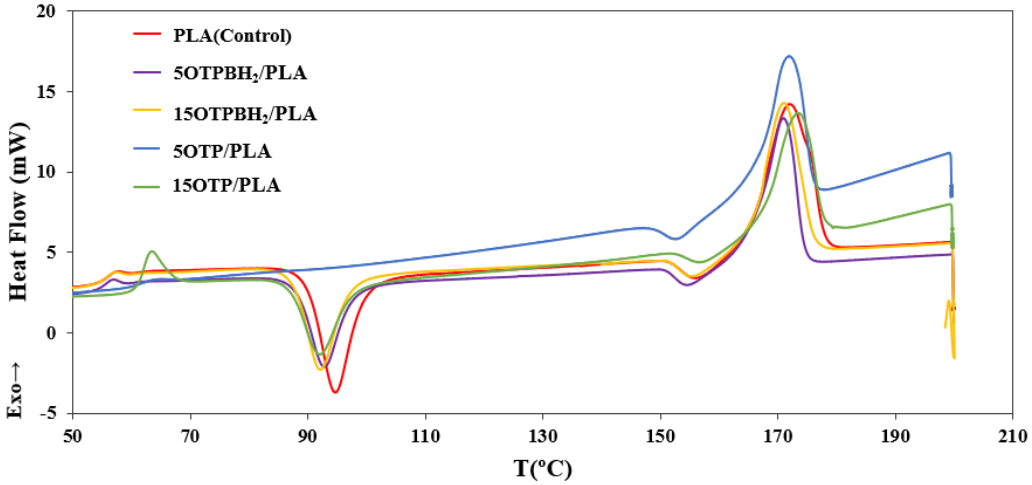

Figure 11. Thermograms resulting from the DSC performed on PLA (Control) and biocomposites.

Addition of OTPBH$_2$ to PLA caused a reduction of ΔH_m by 13.5% compared to pure PLA, since the incorporation of fibres shortens the PLA polymer chains and decreases their mobility [19]. The peaks corresponding to the melting and crystallisation processes changed to lower temperatures after the incorporation of OTP with and without treatment. For the case of the addition of 15 wt.% OTPBH$_2$, T_c decreased from 94.63 °C to 92.08 °C and T_m from 172.0 °C to 171 °C, indicating that both type of OTP, with and without treatment, presented a nucleation effect on the growth of PLA spherulites [53]. In addition, they also act as starting points for crystal growth, resulting in earlier crystallisation of biocomposites, as a consequence of the decrease in T_c. PLA crystallinity increased from 38.44% to 40.44% with the addition of OTPBH$_2$, confirming the role of cellulose as a nucleating agent that promotes PLA crystallisation [59][61]. Also, the extrusion process and the subsequent injection moulding, generated an improvement in the orientation of the fibres and in the molecular orientation of the polymer chains, resulting in the improvement of crystallinity [48].

TGA tests were carried out to analyse the thermal degradation of the PLA(control) and the manufactured biocomposites. Figure 12 and Table 6 shows the loss of mass of the different materials as a function of temperature and the resulting derivative thermogravimetric (DTG). The first mass loss observed in the samples is slight, occurs a little before reaching 100 ºC and can be attributed to the moisture loss of each sample. The main loss of mass of the samples takes place between 300-400 ºC, and corresponds mainly to the degradation of the polymer matrix [62][63]. Td,i begins of the PLA takes place at 331 ºC, decreasing this value with the incorporation of the reinforcement, said decrease being greater in the case of a 15 wt.% reinforcement. The addition of the reinforcement led to a lower degradation temperature of the material and to an increase in the residual mass, as shown in Table 6. No further loss of mass was observed above 500 ºC in any of the samples, indicating that the polymer transformed into char at this point. Those biocomposites fabricated with untreated fibre present a Td,i around 312-326 ºC, while the biocomposites with treated fibre present an extended range between 299-226 ºC. This indicates that the incorporation of fibre causes a decrease in the relative molecular mass of PLA [64]. The residual mass is greater as the percentage of reinforcement increases and the treatment of the fibre is carried out. This is due to the fact that the fibre without treatment, as it contains a higher content of lignin and hemicellulose, generates less residual mass [63]. The decrease in the degradation temperature when incorporating lignocellulosic residues, this being higher after carrying out a cellulose purification treatment, was previously reported by other authors [64].

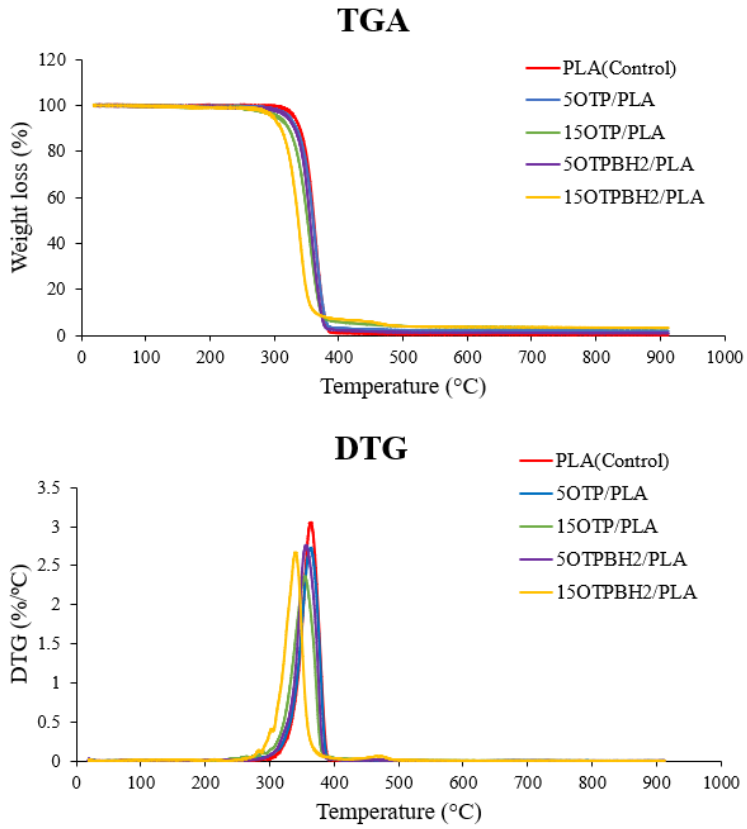

688

689 **Figure 12.** TGA and DTG curves of PLA(Control) and biocomposites.

690 **Table 6.** Thermal properties of PLA and biocomposites obtained from TGA

Material Reference	$T_{d,i}$ (ºC)	$T_{d,max}$ (ºC)	$T_{d,f}$ (ºC)	Solid residue (wt.%)
PLA (Control)	331.21	363.46	380.41	0.12
5OTP/PLA	325.56	363.16	378.11	1.86
5OTPBH$_2$/PLA	325.74	356.32	374.50	0.91
15OTP/PLA	312.79	354.17	371.67	3.16
15OTPBH$_2$/PLA	299.73	340.06	361.19	3.29

691

692 *3.4.4. Water absorption*

693 The results obtained from the c determination tests for the different materials tested are

694 shown in Table 7.

695 **Table 7.** Water absorption properties of PLA and biocomposites

Material Reference	c (%)
PLA (Control)	0.5932±0.0149
5OTP/PLA	1.0210±0.0519
5OTPBH$_2$/PLA	0.6358±0.0281

15OTP/PLA	1.1791±0.0213
15OTPBH_2/PLA	0.7911±0.0065

696

697 The results in the table above corroborate the hydrophobic nature of PLA [64]. From the
698 above data it can also be deduced that the water absorption capacity increases as the fibre
699 weight percentage increases, mainly due to the hydrophilic nature of the fibre as it
700 contains a large amount of -OH groups [62]. Those biocomposites made from treated
701 fibre present a lower c value than those containing untreated fibre. This indicates that the
702 chemical treatment decreases the water absorption capacity of the fibre. The treatment
703 carried out for the purification of the cellulose directly affect the -OH groups of the fibre,
704 decreasing its hydrophilic character, and therefore that of the corresponding
705 biocomposites. This same effect has been reported by other authors after performing an
706 alkaline treatment [64].

707 **4. Conclusions**

708 According to the results presented above, it can be concluded that OTP biomass presents
709 outstanding characteristics in terms of composition to be considered as a suitable source
710 for obtaining cellulose. An efficient procedure for the extraction and purification of
711 cellulose from OTP was successfully developed, this process being based on hydrolysis
712 with HNO_3 followed by subsequent treatment with NaOH. The reaction time, temperature
713 and HNO_3 concentration in the acid hydrolysis reaction were optimised using RSM
714 methodology for the maximisation of hemicellulose and lignin removal, and the
715 minimisation of the cellulose hydrolysis. Subsequent alkaline treatment under specific
716 conditions allowed to obtain a final solid with a high purity in cellulose (83.28 wt.%) and
717 a very low percentage of lignin (5.00 wt.%), whereas the hemicellulose content was
718 practically negligible (0.5 wt.%).

719 The characterisation of the raw OTP fibres and after each treatment by different analytical
720 techniques, namely SEM, FTIR, XRD and TGA, confirmed the changes produced in the
721 chemical composition and structure of raw the OTP fibres as a consequence of the
722 hydrolysis procedure. The cellulosic fraction isolated had high both crystallinity and
723 thermal stability and, therefore, it may be considered for further conversion on cellulose
724 derivatives with application in varied industrial sectors such as papermaking or plastic-
725 related industries.
726 The introduction of high percentages (15 wt.%) of this treated fibre within a PLA matrix
727 to obtain biocomposites implies a significant reduction in tensile strength, so when the
728 percentages introduced are low (5 wt.%), a slight increase in this property can be
729 achieved. When it comes to untreated fibre, elongation at break and impact strength
730 values were significantly reduced in the same way, which was due to the presence of
731 stress concentrators at the fiber-matrix interface. However, the tensile strength values
732 were maintained. The value of the Young's modulus was significantly reduced for low
733 percentages of fibre and increased for high percentages of treated fibre. In general, the
734 reinforcement with OTP did not produce any significant increase in the mechanical
735 properties for any of the reinforcement percentages. The only improvement of the
736 mechanical properties of the tested PLA-based biocomposites occurred when the non-
737 cellulosic compounds were previously removed from the OTP, as a consequence of a
738 better interaction between the fibre and the polymer matrix. The FTIR analyses do not
739 show significant changes in the chemical composition of the biocomposites due to the
740 incorporation of the reinforcements. XRD analyses demonstrate the presence of type I
741 cellulose in the biocomposite with treated fibre. The SEM images obtained from the
742 fracture surfaces of the tested specimen show good fibre-PLA cohesion, being even
743 higher when the $OTPBH_2$ is used. DSC curves obtained indicate that the incorporation of

744 $OTPBH_2$ favours the shortening and reduction of the mobility of the PLA chains, which
745 translates into a reduction of up to 13.5% of AH_m. In addition, there is a slight decrease
746 in both T_c and T_m as a consequence of the OTP, both chemically treated and untreated,
747 has a nucleating effect on the growth of PLA spherulites. Said nucleating effect also gives
748 rise to an increase in the crystallinity values of the material, which are also favoured by
749 the orientation of the polymer molecules that occurs during the extrusion process. The
750 resulting TGA curves shows a slight decrease in the degradation temperature of the
751 biocomposites due to the presence of fibre, this decrease being more significant in the
752 case of treated fibre. The percentage of solid waste at the end of the TGA analysis is lower
753 in the case of biocomposites reinforced with treated fibre, due to the elimination of non-
754 cellulosic components as a result of the chemical treatment. In terms of water absorption
755 capacity, those biocomposites containing untreated fibre present higher values, therefore,
756 the incorporation of fibres with a high cellulose content improves biocomposite
757 hydrophobic tendency.

758 **Data Availability**

759 All data is freely available by contacting the corresponding author.

760 **Acknowledgements**

761 The authors thank the financial support provided by the BIONANOCEL project of
762 Fundación Andaltec I+D+I (Spain) and the technical assistance from CICT (University
763 of Jaén, Spain).

764 **Funding**

765 This work was supported by the regional government of Andalusia (southern Spain)
766 [grant code PY18-RE-0016] through European Regional Development Fund.

767 **Competing Interest**

768 The authors declare that they have no known relevant financial or non-financial interests
769 to disclose that could have influenced the work reported in this paper.

770 **References**

771 [1] Klemm, D, Heublein, B, Fink, HP et al. Cellulose: fascinating biopolymer and
772 sustainable raw material. Angew. Chem. Int. Ed. 2005; 44(22): 3358-3393.
773 https://doi.org/10.1002/anie.200460587.

774 [2] Tezcan, E, Atici, OG. A new method for recovery of cellulose from lignocellulosic
775 bio-waste: Pile processing. Waste Manag. 2017; 70: 181-188.
776 https://doi.org/10.1016/j.wasman.2017.09.017.

777 [3] Dunlop, MJ, Acharya, B, Bissessur, R. Isolation of nanocrystalline cellulose from
778 tunicates. J. Environ. Chem. Eng. 2018; 6(4): 4408-4412.
779 https://doi.org/10.1016/j.jece.2018.06.056.

780 [4] Sheng, S, Meiling, Z, Chen, L, et al. Extraction and characterization of
781 microcrystalline cellulose from waste cotton fabrics via hydrothermal method. Waste
782 Manag. 2018; 82: 139-146. https://doi.org/10.1016/j.wasman.2018.10.023.

783 [5] Kian, LK, Saba, N, Jawaid, M, et al. Properties and characteristics of nanocrystalline
784 cellulose isolated from olive fiber. Carbohydr. Polym. 2020; 241: 116423.
785 https://doi.org/10.1016/j.carbpol.2020.116423.

786 [6] Foo, ML, Ooi, CW, Tan, KW, et al. A step closer to sustainable industrial production:
787 tailor the properties of nanocrystalline cellulose from oil palm empty fruit bunch. J.
788 Environ. Chem. Eng. 2020; 8(5): 104058.
789 https://doi.org/10.1016/j.jece.2020.104058.

790 [7] Sun, JX, Xu, F, Geng, ZC, et al. Comparative study of cellulose isolated by totally
791 chorine-free method from wood and cereal straw. J. Appl. Polym. Sci. 2005; 97(1):
792 322-335. https://doi.org/10.1002/app.21728.

[8] Kim, JS, Lee, YY, Torget, RW. Cellulose hydrolysis under extremely low sulfuric acid and high-temperature conditions. Appl. Biochem. Biotechnol. 2001; 91: 331-340. https://doi.org/10.1385/ABAB:91-93:1-9:331.

[9] Rodríguez-Chong, A, Ramírez, JA, Garrote, G, et al. Hydrolysis of sugar cane bagasse using nitric acid: a kinetic assessment. J. Food Eng. 2004; 61(2): 143-152. https://doi.org/10.1016/S0260-8774(03)00080-3.

[10] Evans, SK, Wesley, ON, Nathan, O, et al. Chemically purified cellulose and its nanocrystals from sugarcane baggase: isolation and characterization. Heliyon 2019; 5: e02635. https://doi.org/10.1016/j.heliyon.2019.e02635.

[11] Trilokesh, C, Uppuluri, KB. Isolation and characterization of cellulose nanocrystals from jackfruit peel. Sci. Rep. 2019; 9: 16709. https://doi.org/10.1038/s41598-019-53412-x.

[12] Morán, JI, Alvarez, VA, Cyras, VP, et al. Extraction of cellulose and preparation of nanocellulose from sisal fibers. Cellulose 2008; 15(1): 149-159. https://doi.org/10.1007/s10570-007-9145-9.

[13] Rosa, MF, Medeiros, ES, Malmonge, JA, et al. Cellulose nanowhiskers from coconut husk fibers: Effect of preparation conditions on their thermal and morphological behaviour. Carbohydr. Polym. 2010; 81(1): 83-92. https://doi.org/10.1016/j.carbpol.2010.01.059.

[14] Cavali, M, Soccol, CR, Tavares, D, et al. Effect of sequential acid-alkaline treatment on physical and chemical characteristics of lignin and cellulose from pine (Pinus spp.) residual sawdust. Bioresour. Technol. 2020; 316: 123884. https://doi.org/10.1016/j.biortech.2020.123884.

816 [15] Vadivel, V, Moncalvo, A, Dordoni, R, et al. Effects of an acid/alkaline treatment on
817 the release of antioxidants and cellulose from different agro-food wastes. Waste
818 Manag. 2017; 64: 305-314. https://doi.org/10.1016/j.wasman.2017.03.010.
819 [16] Agencia Andaluza de la Energía (2020).
820 https://www.agenciaandaluzadelaenergia.es/sites/default/files/Documentos/3_2_00
821 68_20_LA_BIOENERGIA_EN_ANDALUCIA.PDF. Last accessed December
822 2021.
823 [17] Njeh, F, Hamza, M, Bouaziz, I, et al. Isolation, characterization and methylene blue
824 adsorption: Application of cellulose from olive sawdust. Korean J. Chem. Eng. 2022;
825 39: 760-774. https://doi.org/10.1007/s11814-021-0931-0.
826 [18] Kian, LK, Saba, N, Jawaid, M, et al. Characterization of microcrystalline cellulose
827 extracted from olive fiber. Int. J. Biol. Macromol. 2020; 156: 347-353.
828 https://doi.org/10.1016/j.ijbiomac.2020.04.015.
829 [19] Bhasney, SM, Mondal, K, Kumar, A, et al. Effect of microcrystalline cellulose
830 [MCC] fibres on the morphological and crystalline behaviour of high density
831 polyethylene [HDPE]/polylactic acid [PLA] blends. Compos. Sci. Technol. 2019;
832 187(3): 107941. https://doi.org/107941. 10.1016/j.compscitech.2019.107941.
833 [20] Kumar, KN, Babu, PD, Surakasi, R, et al. Mechanical and Thermal Properties of
834 Bamboo Fiber–Reinforced PLA Polymer Composites: A Critical Study. Int. J.
835 Polym. Sci. 2022; 2022. https://doi.org/10.1155/2022/1332157.
836 [21] Fico, D, Rizzo, D, Carolis, V, et al. Development and characterization of sustainable
837 PLA/Olive wood waste composites for rehabilitation applications using Fused
838 Filament Fabrication (FFF). J. Build. Eng. 2022; 56: 104673.
839 https://doi.org/10.1016/j.jobe.2022.104673.

840 [22] AL-Oqla, F. Predictions of the Mechanical Performance of Leaf Fiber Thermoplastic
841 Composites by FEA. Int. J. Appl. Mech. 2021; 13: 2150066
842 https://doi.org/10.1142/S1758825121500666.
843 [23] Sarmin, SN, Jawaid, M, Mahmoud, M, et al. Mechanical and physical properties
844 analysis of olive biomass and bamboo reinforced epoxy-based hybrid composites.
845 Biomass Convers. Biorefin. 2022; https://doi.org/10.1007/s13399-022-02872-9.
846 [24] Termizi, M, Rasidi, M, Zainuddin, F, et al. Mechanical and morphological properties
847 of pure α-cellulose-filled polylactic acid (PLA) biocomposite. AIP Conf. Proc. 2022;
848 2496: 020008. https://doi.org/10.1063/5.0090708.
849 [25] Nurazzi, NM, Abdullah, N, Norrrahim, MNF, et al. Thermogravimetric Analysis
850 (TGA) and Differential Scanning Calorimetry (DSC) of PLA/Cellulose Composites.
851 In: Polylactic Acid-Based Nanocellulose and Cellulose Composites. 1st ed. 2022, pp.
852 145-163. https://doi.org/10.1201/9781003160458-7.
853 [26] Mateo, S, Puentes, JG, Roberto, IC, et al. Optimization of acid hydrolysis of olive
854 tree pruning residue. Fermentation with Candida guilliermondii. Biomass and
855 bioenergy 2014; 69: 39-46. https://doi.org/10.1016/j.biombioe.2014.07.007.
856 [27] Browning, BL. Determination of lignin. In: Browning, BL (eds). *Methods of wood*
857 *chemistry*. Wiley & Sons, New York 1967, vol. I, pp. 785-823.
858 [28] Irick, TJ, West, K, Brownell, HH, et al. Comparison of colorimetric and HPLC
859 techniques for quantitating the carbohydrate components of steam-treated wood.
860 Appl. Biochem. Biotechnol. 1988; 17(1): 137-149.
861 https://doi.org/10.1007/BF02779152.
862 [29] Rocha, GJM. *Deslignificaçao de bagaço de cana de azúcar assistida por oxigênio*.
863 PhD, University of São Paolo, Brazil, 2000.

[30] Segal, L, Creely, JJ, Martin, AE, et al. An Empirical Method for Estimating the Degree of Crystallinity of Native Cellulose Using the X-Ray Diffractometer. Text. Res. J. 1959; 29(10). https://doi.org/10.1177/004051755902901003.

[31] Johar, N, Ahmad, I, and Dufresne, A. Extraction, preparation and characterization of cellulose fibres and nanocrystals from rice husk. Ind. Crops Prod. 2012; 37(1): 93–99. https://doi.org/10.1016/j.indcrop.2011.12.016.

[32] Kassab, Z, Abdellaoui, Y, Salim, MH, et al. Micro- and nano-celluloses derived from hemp stalks and their effect as polymer reinforcing materials. Carbohydr. Polym. 2020; 245: 116506. https://doi.org/10.1016/j.carbpol.2020.116506.

[33] Tanpichai, S, Witayakran, S, and Boonmahitthisud, A. Study on structural and thermal properties of cellulose microfibers isolated from pineapple leaves using steam explosion. J. Environ. Chem. Eng. 2018; 7(1): 102836. https://doi.org/10.1016/j.jece.2018.102836.

[34] Jurado-Contreras, S, Navas-Martos, FJ, Rodríguez-Liébana, et al. Manufacture and Characterization of Recycled Polypropylene and Olive Pits Biocomposites. Polymers 2022, 14, 4206. https://doi.org/10.3390/polym14194206.

[35] UNE-EN ISO 527-2:2012. Plastics - Determination of tensile properties - Part 2: Test conditions for moulding and extrusion plastics.

[36] UNE-EN ISO 179-1:2011. Plastics - Determination of charpy impact properties - part 1: noninstrumented impact test.

[37] Dong, Y, Ghataura, A, Takagi, H, et al. Polylactic acid (PLA) biocomposites reinforced with coir fibres: Evaluation of mechanical performance and multifunctional properties. Compos. - A: Appl. Sci. Manuf. 2014; 63: 76–84. https://doi.org/10.1016/j.compositesa.2014.04.003.

[38] UNE-EN ISO 62:2008. Plastics - Determination of water absorption

[39] Mateo, S, Roberto, IC, Sánchez, S, et al. Detoxification of hemicellulosic hydrolyzate from olive tree pruning residue. Ind. Crops Prod. 2013; 49: 196–203. https://doi.org/10.1016/j.indcrop.2013.04.046.

[40] Negro, MJ, Duque, A, Manzanares, P, et al. Alkaline twin-screw extrusion fractionation of olive-tree pruning biomass. Ind. Crops Prod. 2015; 74: 336-341. https://doi.org/10.1016/j.indcrop.2015.05.018.

[41] Requejo, A, Rodríguez, A, Colodette, JL, et al. Optimization of ECF bleaching and refining of kraft pulping from olive tree pruning. Bioresources 2012; 7(3): 4046-4055.

[42] Sánchez-Gutiérrez, M, Espinosa, E, Bascón-Villegas, I, et al. Production of Cellulose Nanofibers from Olive Tree Harvest-A Residue with Wide Applications. Agronomy 2020; 10(5): 696. https://doi.org/10.3390/agronomy10050696.

[43] Melikoğlu, AY, Bilek, SE, and Cesur, S. Optimum alkaline treatment parameters for the extraction of cellulose and production of cellulose nanocrystals from apple pomace. Carbohydr. Polym. 2019; 215: 330-337. https://doi.org/10.1016/j.carbpol.2019.03.103.

[44] Neto, BB, Scarminio, IS, and Bruns, RE. Empirical model-building. In: Bruns RE, Neto, BB (eds) *Data handling in science and technology*, Elsevier Science 2005a.

[45] Trinh, HT, Duong, HT, Ta, TT, et al. Simultaneous effect of dissolved organic carbon, surfactant, and organic acid on the desorption of pesticides investigated by response surface methodology. Environ. Sci. Pollut. Res. 2017; 24: 19338–19346. https://doi.org/10.1007/s11356-017-9431-5.

[46] Jiménez, L, Pérez, I, de la Torre, MJ, et al. The effect of processing variables on the soda pulping of olive tree wood. Bioresour. Technol. 1999; 69(2): 95-102. https://doi.org/10.1016/S0960-8524(98)00183-7.

914 [47] Dou, J, Karakoç, A, Johansson, LS, et al. Mild alkaline separation of fiber bundles
915 from eucalyptus bark and their composites with cellulose acetate butyrate. Ind. Crops
916 Prod. 2021; 165: 113436. https://doi.org/10.1016/j.indcrop.2021.113436.
917 [48] Zhou, L, He, H, Jiang, C, et al. Cellulose nanocrystals from cotton stalk for
918 reinforcement of poly(vinyl alcohol) composites. Cellul. Chem. Technol. 2017; 51:
919 109-119.
920 [49] Elyamine, AM, Moussa, MG, Afzal, J, et al. Modified rice straw enhanced cadmium
921 (II) immobilization in soil and promoted the degradation of phenanthrene in co-
922 contaminated soil. Int. J. Mol. Sci. 2019; 20(9).
923 https://doi.org/10.3390/ijms20092189.
924 [50] Luzi, F, Fortunati, E, Puglia, D, et al. Optimized extraction of cellulose nanocrystals
925 from pristine and carded hemp fibres. Ind. Crops Prod. 2014; 56: 175-186.
926 https://doi.org/10.1016/j.indcrop.2014.03.006.
927 [51] Akinjokun, AI, Petrik, LF, Ogunfowokan, AO, et al. Isolation and characterization
928 of nanocrystalline cellulose from cocoa pod husk (CPH) biomass wastes. Heliyon
929 2021; 7(4). https://doi.org/10.1016/j.heliyon.2021.e06680.
930 [52] Sangeetha, VH, Varghese, TO, Nayak, SK. Value Addition of Waste Cotton: Effect
931 of Nanofibrillated Cellulose on EVA/EVOH Toughened Polylactic Acid System.
932 Waste Biomass Valorization 2020, 11, 4119-4128. https://doi.org/10.1007/s12649-
933 019-00738-2.
934 [53] Bhasney, SM, Bhagabati, P, Kumar, A, et al. Morphology and crystalline
935 characteristics of polylactic acid [PLA]/ linear low density polyethylene [LLDPE]/
936 microcrystalline cellulose [MCC] fiber composite. Compos. Sci. Technol. 2018; 171:
937 54-61. https://doi.org/10.1016/j.compscitech.2018.11.028.

938 [54] Benyahia, A, Merrouche, A, Rahmouni, Z, et al. Study of the alkali treatment effect
939 on the mechanical behavior of the composite unsaturated polyester-Alfa fibers.
940 Mech. Ind. 2014; 15(1): 69-73. https://doi.org/10.1051/meca/2013082.
941 [55] Naghmouchi, I, Mutjé, P, and Boufi, S. Olive stones flour as reinforcement in
942 polypropylene composites: a step forward in the valorization of the solid waste from
943 the olive oil industry. Ind. Crops Prod. 2015; 72: 183-191.
944 https://doi.org/10.1016/j.indcrop.2014.11.051.
945 [56] Bhiogade, A and Kannan, M. Studies on thermal and degradation kinetics of cellulose
946 micro/nanoparticle filled polylactic acid (PLA) based nanocomposites. Polym.
947 Polym. Compos. 2021; 29. https://doi.org/10.1177/0967391120987170.
948 [57] Chieng, BW, Ibrahim, NA, Yunus, W, et al. Effects of Graphene Nanopletelets on
949 Poly(Lactic Acid)/Poly(Ethylene Glycol) Polymer Nanocomposites. Polymers 2013;
950 6: 93-104. https://doi.org/10.3390/polym6010093.
951 [58] Komal, U, Lila, M, and Singh, I. PLA/banana fiber based sustainable biocomposites:
952 A manufacturing perspective. Compos. B. Eng. 2019; 180: 107535.
953 https://doi.org/107535. 10.1016/j.compositesb.2019.107535.
954 [59] Bhasney, S, Kumar, A, and Katiyar, V. Microcrystalline cellulose, polylactic acid
955 and polypropylene biocomposites and its morphological, mechanical, thermal and
956 rheological properties. Compos. B. Eng. 2019; 184: 107717.
957 https://doi.org/10.1016/j.compositesb.2019.107717.
958 [60] Yu, T, Ren, J, Li, S, et al. Effect of fiber surface-treatments on the properties of
959 poly(lactic acid)/ramie composites. Compos. Part A Appl. 2010; 41(4): 499-505.
960 https://doi.org/10.1016/j.compositesa.2009.12.006.

961 [61] Zhang, Q, Lei, H, Cai, H, et al. Improvement on the properties of microcrystalline
962 cellulose/polylactic acid composites by using activated biochar. J. Clean. Prod. 2019;
963 252(8): 119898. https://doi.org/10.1016/j.jclepro.2019.119898.
964 [62] Diyana, AF, Khalina, A, Sapuan, MS, et al. Physical, Mechanical, and Thermal
965 Properties and Characterization of Natural Fiber Composites Reinforced Poly(Lactic
966 Acid): Miswak (Salvadora Persica L.) Fibers. Int. J. Polym. Sci. 2022: 2022.
967 https://doi.org/10.1155/2022/7253136.
968 [63] Bajpai, PK, Singh, I and Madaan, J. Tribological behavior of natural fiber reinforced
969 PLA composites. Wear 2013; 297 (1-2): 829-840.
970 https://doi.org/10.1016/j.wear.2012.10.019.
971 [64] Gunti, Ra, Prasad, AV, and Gupta, A. Mechanical and degradation properties of
972 natural fiber reinforced PLA composites: Jute, sisal, and elephant grass: Mechanical
973 and Degradation Properties of Natural Fiber Reinforced PLA Composites. Polymer
974 Composites. 2016; 39: 1125-1136. https://doi.org/10.1002/pc.24041.
975